Tectonophysics 760 (2019) 36–57

Contents lists available at ScienceDirect

Tectonophysics

journal homepage: www.elsevier.com/locate/tecto

Large-scale rotations of the Chortis Block (Honduras) at the southern termination of the Laramide flat slab

Roberto S. Molina Garza[a,*], Douwe J.J. van Hinsbergen[b], Lydian M. Boschman[b], Robert D. Rogers[c], Morgan Ganerød[d]

[a] Centro de Geociencias, Universidad Nacional Autónoma de México, Blvd. Juriquilla 3001, Querétaro, Mexico
[b] Department of Earth Sciences, Utrecht University, Heidelberglaan 2, 3584 CS Utrecht, Netherlands
[c] Department of Physics and Geology, California State University, Stanislaus, 801 W. Monte Vista Ave., Turlock, CA, USA
[d] Geological Survey of Norway NGU, Leiv Eirikssons Vei 39, 7491 Trondheim, Norway

ARTICLE INFO

Keywords:
Honduras
Chortis
Mexico
Laramide
Caribbean
Cretaceous

ABSTRACT

Paleogeographic reconstructions place the Chortis block adjacent to southern Mexico in the Late Cretaceous and earlier time, forming the tectonically disturbed southwestern tip of the North American plate. This study assesses the relative motion between Chortis and North America during the Laramide orogeny, later development of the North America-Caribbean plate boundaries. We carried out paleomagnetic analysis of rotations and latitudinal displacement using a total of 90 sites from the Átima Limestone and the Valle de Ángeles Formation redbeds sampled at seven localities in Honduras. Two secondary but ancient magnetizations post-date Late Cretaceous folding at most localities. The oldest magnetization is a ChRM of high laboratory unblocking temperature in the redbeds (> 650 °C), and a moderate temperature in the limestones (500–600 °C). This component is WNW directed at five localities, varying somewhat in declination, having a consistent moderate positive inclination (mean $I = 39.7°$; $\alpha95 = 6.8°$, $n = 53$ sites). The age of the ChRM is bracketed between 85 and 63 Ma, based on youngest zircon age and the age of a cross-cutting dike. An intermediate unblocking temperature component present in both units (Dec = 146.2°, Inc = −28.5°; k = 13.1, $\alpha95 = 6.8°$, $n = 37$ sites), is interpreted as an overprint. The ChRM indicates an average counterclockwise rotation of 55.4 ± 5.7°, with respect to the expected direction. The younger overprint was acquired between ~50 and 15 Ma; its mean is also discordant with the expected North America direction, implying some Neogene rotation of Chortis. Abundant late Albian-Turonian zircons in Valle de Ángeles redbeds explicitly require extending the Laramide arc along western Mexico into Chortis. A reconstruction of Chortis south of Mexico that takes into account 55 degrees of rotation shows a gap between both continental blocks at about 70 Ma. We propose a model where this gap formed by back-arc extension creating the Late Cretaceous Chontal basin at the southern termination of the Laramide flat-slab.

1. Introduction

The plate kinematic history of the eastern Paleo-Pacific realm poses intriguing questions on the relationships between subduction processes and crustal deformation. While convergence between the plates of the Paleo-Pacific realm (or Panthalassa) and North and South America probably had an eastward vergence in Cretaceous time, the segment in between the Americas was characterized by westward subduction of North and South American ('Proto-Caribbean') oceanic lithosphere below a portion of trapped Panthalassa lithosphere that became the Caribbean plate (CAR) (e.g., Pindell and Kennan, 2009; Boschman et al., 2014). The style of convergence and deformation associated with these subduction segments has been very different. In particular, the subduction segments beneath the Americas have undergone (and are undergoing) episodes of flat-slab subduction, which led to significant deformation. Examples include the Laramide flat-slab episode which is responsible the Laramide orogeny and the Sierra Madre foldbelt between ~80 and 50 Ma (Bird, 1988; DeCelles et al., 2009; Liu et al., 2010; Fitz-Díaz et al., 2011).

The eastward-verging Laramide flat-slab formed at the North America (NAM)-Farallon (FAR) trench, which to the south must have ended in a triple junction where it met the CAR boundaries (Fig. 1). In Late Cretaceous and younger time, the northern and eastern CAR had an opposite westward-dipping subduction zone at the CAR-NAM and CAR-South American plate (SAM) boundaries. This convergent margin had formed around ~130 Ma; an eastward dipping subduction zone

* Corresponding author.
E-mail address: rmolina@geociencias.unam.mx (R.S. Molina Garza).

https://doi.org/10.1016/j.tecto.2017.11.026
Received 6 June 2017; Received in revised form 31 October 2017; Accepted 19 November 2017
Available online 24 December 2017
0040-1951/

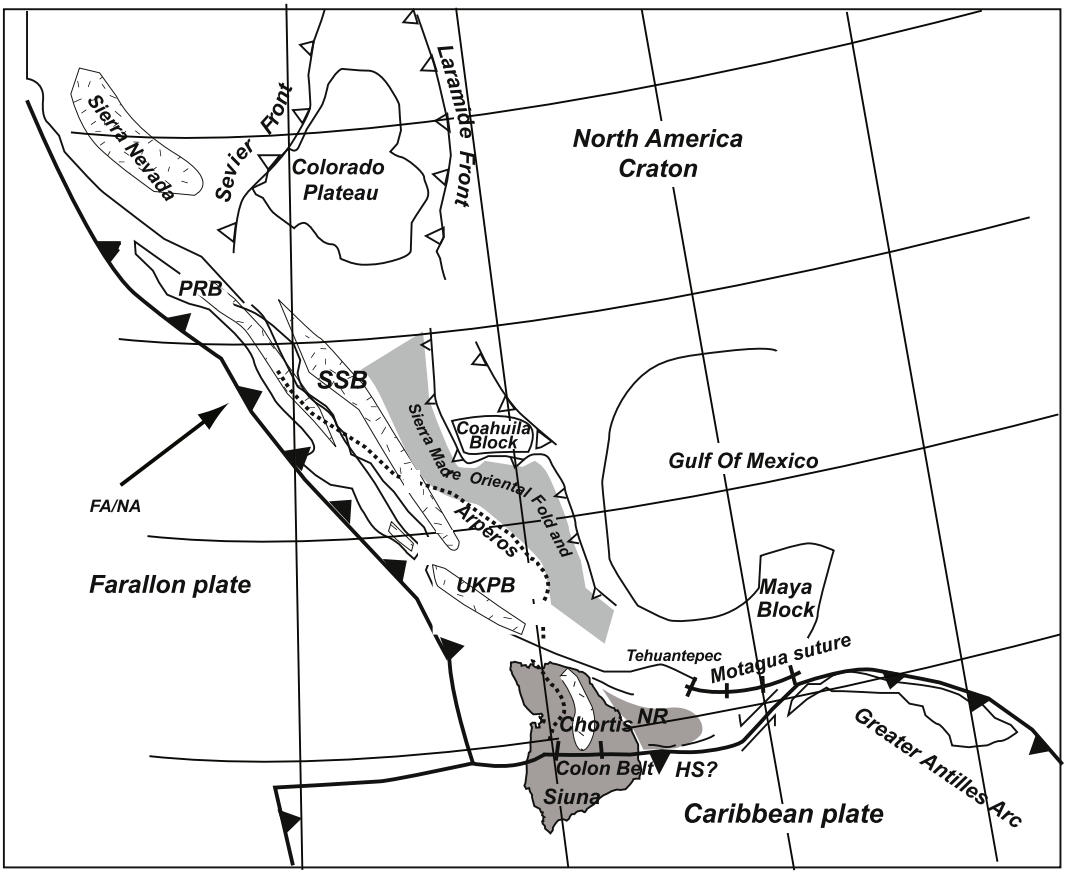

Fig. 1. Tectonic scenario for the southern termination of the Laramide systems at about 70 Ma and the region of interaction between the Caribbean, Farallon and North America plates. The figure shows Cretaceous plutonism and major Cretaceous mountain building systems: the Sevier front and the Laramide front in western USA, and the Early Cretaceous Arperos suture and the Laramide age Sierra Madre Oriental fold and thrust belt. The position of the Sierra Madre Oriental in a back arc setting is evident. Other Cretaceous sutures are the Colon Belt and the Motagua region of Guatemala. A reconstruction shows the Chortis block off-southern Mexico (after Rogers et al., 2007a), and the Greater Antilles Arc colliding with the Maya Block. PRB is the Peninsular Ranges Batholith, SSB is the Sonora-Sinaloa batholith, and UKPB is the Early-Late Cretaceous Puerto Vallarta and Manzanillo batholith. HS? Is a possible plate boundary at the Hess Escarpment and NR is the Nicargua rise.

formed at its western boundary with FAR (Pindell and Kennan, 2009; Lázaro et al., 2009; Boschman et al., 2014). Plate reconstructions show that the FAR-CAR trench must have been offset to the west of the FAR-NAM trench (Pindell and Kennan, 2009; Boschman et al., 2014), from which it follows that the Laramide flat-slab must have had a slab edge in the south (Fig. 1).

The kinematic and geodynamic history of the southern termination of the flat slab that is thought to have created the Laramide orogeny may reside in a continental fragment that now is part of the Caribbean plate: the Chortis block. Today the Chortis block occupies much of Guatemala, El Salvador and Honduras (Fig. 2). The Chortis block was captured by the Caribbean plate when the modern Caribbean-North American transform plate boundary formed. This plate boundary is a left-lateral transform plate boundary along which the Cayman pull-apart basin formed since ~50 Ma (Leroy et al., 2000). This plate boundary extends westward to the Motagua fault zone that separates Chortis from continental Mexico (e.g., Pindell and Kennan, 2009). Prior to ~50 Ma, however, Chortis is generally considered to be part of the deforming southern boundary of the North American plate. Caribbean-North American relative plate motion was accommodated along another transform-dominated plate boundary that may have coincided with the Hess escarpment (Boschman et al., 2014; Mann, 2007; Fig. 1). This places Chortis at the southern termination of the FAR-NAM trench, above which the Sevier, Laramide and Sierra Madre retro-arc fold and thrust belts of western North America formed between 85 and 50 Ma. Alternative models dislodged Chortis from North America during Maastrichtian time due to partial coupling with the eastward moving Caribbean plate (Pindell and Kennan, 2009).

For the tectonic history of Chortis before 50 Ma, several hypotheses have been formulated that have different predictions for the kinematic and dynamic history of this southern termination of the Laramide subduction zone. In its simplest form, Chortis moved parallel to the modern coast of southern Mexico and the modern trace of the Motagua Fault Zone after 50 Ma; before that time was an integral part of North America (e.g. Dengo, 1985; Riller et al., 1992; Herrmann et al., 1994; Ross and Scotese, 1988; Pindell and Barrett, 1990; Meschede and Frisch, 1998; Boschman et al., 2014). This scenario predicts that Chortis underwent a counterclockwise vertical axis rotation equal to the angle between the southern Mexican margin and the Motagua fault of ~25°. On the other hand, Rogers et al. (2007a) suggested that a prominent magnetic anomaly across western Honduras coincides with the Arperos suture between the Guerrero arc(s) and continental North America in Mexico where a similar magnetic anomaly exists. Aligning the magnetic anomaly with the suture would suggest a much larger counterclockwise rotation of ~50–60°, and would require a pre-50 Ma deformation history between Chortis and Mexico during the later stages of the Laramide orogeny. Finally, models exist that treat Chortis as an independent microcontinent with an enigmatic history somewhere in the Panthalassa ocean, but with negligible rotation to reach its present position (Keppie and Moran-Zenteno, 2005); or models that even propose Chortis once occupied a position in the interior of the Gulf of Mexico (Keppie and Keppie, 2012).

To resolve the Cretaceous to Paleocene kinematic history of North America-Caribbean junction, we report new paleomagnetic results from

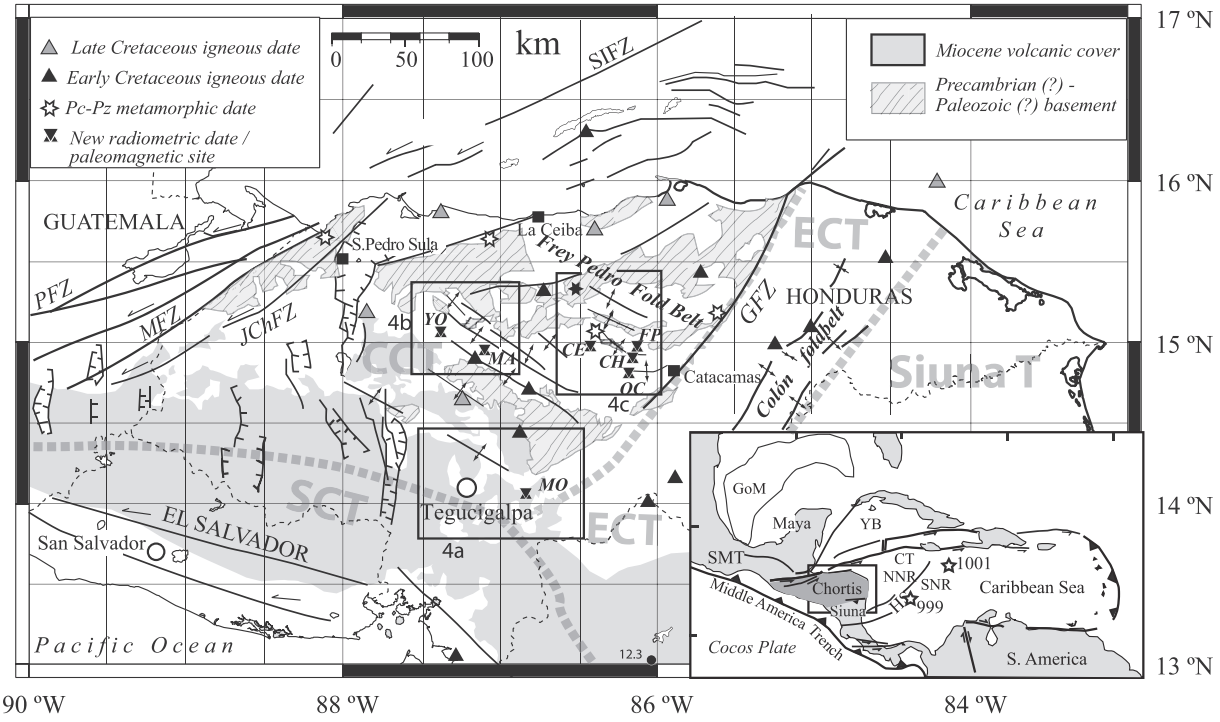

Fig. 2. Schematic tectonic map of the Chortis block (location in the inset), with the distributuion of terranes, metamorphic basement, major strike slip and normal faults, fold trends in Cretaceous strata and geochronological data. SCT = Southern Chortis Terrane; CCT = Centra Chortis Terrane; ECT = Eastern Chortis Terrane; PFZ = Polochic Fault; MFZ = Motagua Fault; JChFZ = Jocotan-Chamalecón Fault; SIFZ = Swan Islands Fault Zone; GFZ = Guayape Fault. Inset: NNR = Northern Nicaragua Rise; SNR = Southern Nicaragua Rise; HS = Hess Ecarpment. After Rogers et al. (2007c).

Cretaceous sedimentary rocks (limestones and redbeds) of Chortis. We provide new $^{40}Ar-^{39}Ar$ ages of volcanic rocks associated with these sediments to provide age control. We also provide a new U/Pb detrital zircon analysis for age constraints and as a first-order test on correlations with Mexican terranes. Using these data we evaluate the rotation history of Chortis, and its implications for its kinematic independence relative to the North American and Caribbean plates as well as the dynamic history of the southern termination of the Laramide flat slab.

2. Geological setting and sampling

The Chortis is a continental block with heterogeneous Precambrian-Paleozoic-Mesozoic metamorphic basement disconformably overlain by Mesozoic and Cenozoic sedimentary and volcanic rocks (Fig. 2; Rogers et al., 2007a). Dengo (1969) defined the Chortis Block as the area of northern Central America, which lies south of the Motagua fault zone. Dengo (1969) placed the southern boundary at about 12.5° N; it may be best placed at the Colon foldbelt (Rogers et al., 2007b), which records the collision of the Siuna assemblage (Fig. 2, inset). The Siuna terrane is an oceanic assemblage accreted to Chortis in the Cretaceous forming a fold and thrust belt that includes ophiolitic elements (Rogers et al., 2007b; Flores et al., 2015). Portions of the Nicaraguan Rise (Fig. 2, inset) may be included in the continental Chortis Block (Case and Holcombe, 1980), but the nature of the rise crust is poorly constrained. Rogers et al. (2007a) recognized that Chortis is a heterogenous block, which includes continental as well as oceanic domains. Chortis contains major crustal discontinuities such as the Guayape fault (Fig. 2).

Previous paleomagnetic investigations have been interpreted to indicate that Chortis moved independently from neighboring blocks in Mexico and the Caribbean in the Cretaceous (Gose, 1985). According to Gose (1985) the Chortis Block experienced a complex rotation history, including both clockwise and counterclockwise rotation. Despite the extensive study, with 37 paleomagnetic sites in a variety of lithologies of mostly Cretaceous age, the complex rotation interpretation presented by Gose (1985) is questionable. This is in part because the Gose (1985) study does not comply with modern analytical standards; although some demagnetization diagrams are presented, there are generally few steps in the demagnetization diagrams. Also a fold test was not quantified. This makes identification of multiple components of magnetization, and the verification of a primary nature of that magnetization, difficult at best.

Our paleomagnetic data were obtained from the widespread Aptian-Albian Átima Limestone and Upper Cretaceous-Paleogene Valle de Ángeles Formation in east-central Honduras, in the region assigned to the Central Chortis terrane (Rogers et al., 2007a). Our motivation to revisit these units is as follows. First, the geodynamic interpretation of paleomagnetic directions presented by Gose (1985) implies that CW rotation of Chortis occurred during deposition of the Átima sequence in the Early Cretaceous, while CCW Chortis rotation occurred during deposition of the Valle de Ángeles Group in the Late Cretaceous. During these intervals Chortis was probably attached to southern Mexico (Rogers et al., 2007a; Silva-Romo, 2008), where such large rotations are not observed (e.g., Molina-Garza et al., 2003; Böhnel et al., 1989). Furthermore, the stratigraphic record shows that the Chortis block was a region of minimal tectonic activity during the mid-Cretaceous. Secondly, most of the sites reported in Gose (1985) are near the southern termination of the San Pedro Sula graben (Fig. 2), in a region in which according to Rogers et al. (2007a) there is a component of transtension associated with the modern North America-Caribbean plate boundary. Tectonic rotation about a local-vertical axis is thus suspected. Finally, Gose's interpretation is based on assigning systematic age differences to Valle de Ángeles strata from different areas without absolute dates, and assuming that paleo-secular variation is averaged at the site level.

2.1. Chortis stratigraphy

The age of basement rocks in Chortis is not well known, but it is generally referred to as pre-Mesozoic based on the limited geochronology available and also because Jurassic strata are the oldest supracrustal rocks yet recognized (Ratschbacher et al., 2009; Finch, 1981;

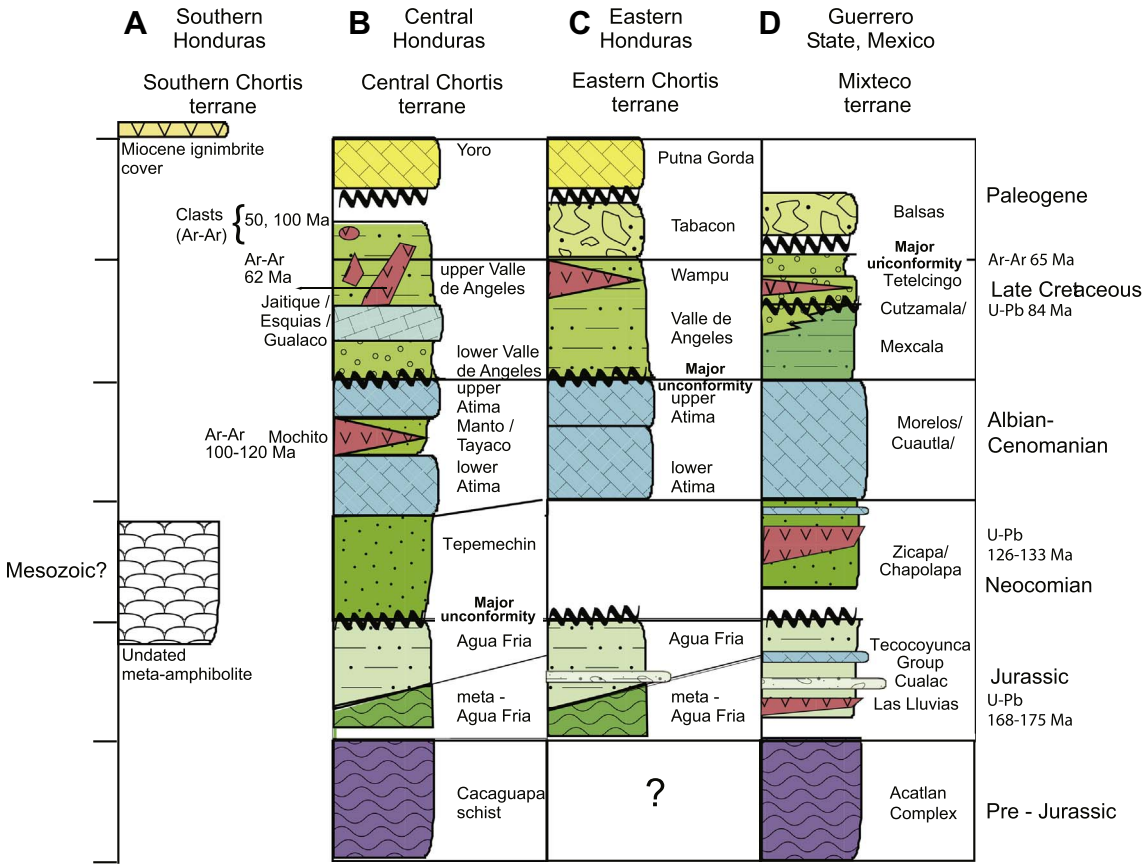

Fig. 3. Revised correlation of Mesozoic strata in the Eastern and Central Chortis terranes with southern Mexico, after Rogers et al. (2007a).

Fig. 3). Basement rocks include gneisses of inferred Mesoproterozoic age (Manton, 1996), and schist of inferred Paleozoic age mostly included in the Cacaguapa Schist. The Cacaguapa Schist mainly consist of low-grade metasedimentary rocks, including phyllite, graphite schist, quartzite, marble, mica schist, and minor metavolcanic rocks. Subordinate amphibolite, greenschist, metagranite, and higher grade rocks have also been reported (e.g., Horne et al., 1976; Simonson, 1977).

The Chortis block cover includes Jurassic, Cretaceous, and minor Paleogene sedimentary rocks overlain by Neogene silicic volcanic rocks (Fig. 3). The oldest strata include the Middle Jurassic ammonite-bearing Agua Fría Formation (Gordon, 1993), as well as unnamed Middle (?) Jurassic continental strata hundreds of meters in thickness consisting of quartz-pebble conglomerate and compositionally mature sandstone. This sequence of continental rocks is associated with siliceous tuff, coal, and plant fossils (R. Rogers, unpublished data). Cretaceous strata include a basal conglomerate and other continental strata of the Tepemechin Formation, a Lower Cretaceous carbonate platform represented by the Lower and Upper Átima Limestones (forming the Yojoa Group), and an Upper Cretaceous dominantly clastic continental sedimentary sequence that contains thin marine units; all are included in the Valle de Ángeles Formation (Rogers et al., 2007a). Cretaceous volcanic rocks are included in the Manto Volcanics (Fig. 3), which separate the Lower and Upper Átima Limestone. The Átima carbonate platform covered most of north-central Honduras, but has not been recognized southeast of the Guayape fault. Platform rim rudist reefs were recognized north of Catacamas at Chocolate Hill. The Upper Átima has been correlated with the mid-Cretaceous Morelos limestone in southern Mexico (Rogers et al., 2007a). Some plutonic rocks recognized in central Honduras provide ages ranging from the Permian to the Paleogene, with common Cretaceous plutons (Fig. 2; Ratschbacher et al., 2009).

Volcanic rocks in the Chortis stratigraphy are a small component. Its significance, however, was recognized by Rogers et al. (2007c) as part of a Lower Cretaceous continental arc. Volcanic and pyroclastic rocks of the Manto Formation are calc-alkaline, and geochemically of arc affinity. Peri-arc sedimentation can be recognized in the volcaniclastic rocks of the Lower Cretaceous Tayaco Formation of the Agalta range (Rogers et al., 2007c), where it underlies the Upper Átima. Cretaceous volcanic rocks have also been reported in the El Porvenir area (Simonson, 1977) and the Catacamas valley (Finch, 1981). Peri-arc sedimentation has also been proposed for the Lower Cretaceous Atzompa, Zicapa and Chivillas Formations in southern Mexico (Sierra-Rojas et al., 2016), which underlie Albian carbonate rocks and have been correlated with the Tayaco and Tepemechin formations in Honduras (Sierra-Rojas et al., 2016).

The Valle de Ángeles Formation overlies the Upper Átima limestones, and it is divided into upper and lower redbeds separated by laterally discontinuous marine limestones (Fig. 3). It is as much as 3000 m in thickness (Finch, 1981). The redbeds crop out throughout a wide region, mostly in south-central Honduras. They are also thought to correlate with Upper Cretaceous rocks in western Mexico such as the Cerro la Vieja and Cutzamala formations. Cenomanian-Turonian limestones within the Valle de Angeles Group have been assigned to the Jaitique, Gualaco and Esquías formations (Finch, 1981; Rogers et al., 2007c). The upper age limit for the Valle de Ángeles Group has not been definitively established. Palynological and paleomagnetic results were used to suggest that the youngest deposits are Campanian (Gose and Finch, 1992); the geochronological data presented later in this paper suggest, however, that it may be as young as Eocene.

Contractional deformation in Honduras was probably synchronous with, or may in part pre-date, deposition of the Valle de Angeles Formation because its general character is similar to molasse deposits. Also, older Cretaceous sedimentary rocks are folded and faulted, but Rogers et al. (2007c) report a slight angular unconformity between

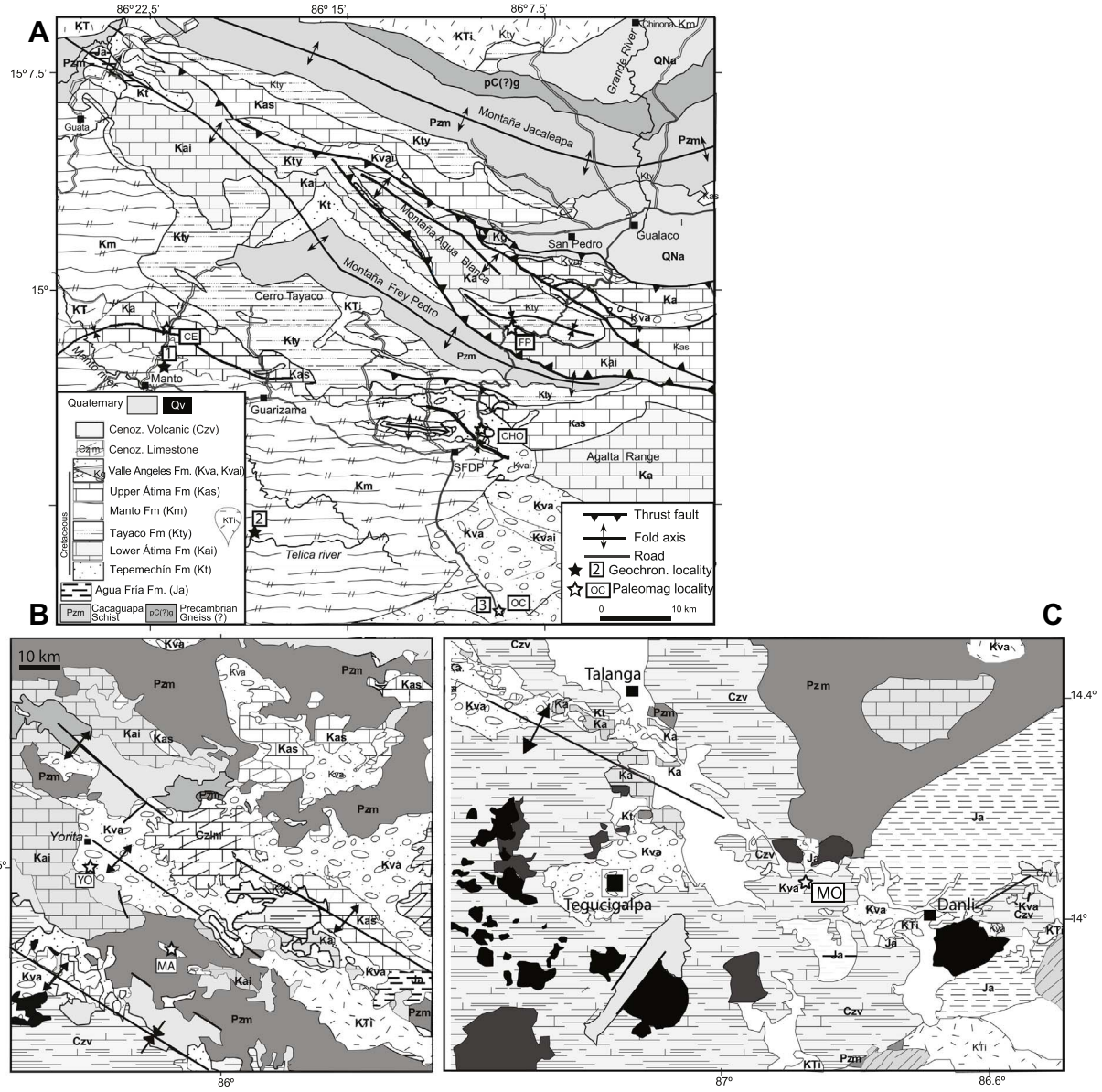

Fig. 4. Geologic maps with sampling localities in the Frey Pedro Mountain area (a and b) and the Moroceli area (c).

Valle de Ángeles and underlying limestones. In the Frey Pedro Mountains, the Valle de Ángeles Formation is folded forming tight upright folds showing clear evidence for post, or late syn-depositional contraction (Rogers et al., 2007c).

2.2. Sampling and methods

We collected paleomagnetic samples from road cuts and natural outcrops in central Honduras (Fig. 4). Samples were drilled in the field with a gas powered portable drill, and oriented in-situ with a magnetic compass as well as an inclinometer. Each site was collected at a single bed, and samples were collected in stratigraphic sequence to increase the chance of sampling across a magnetic reversal. The Valle de Ángeles redbeds were sampled at four localities (Ocote-OC, Moroceli-MO, Marale-MA, and Yoro-YO; Figs. 2 and 4), while samples of the Átima Limestone were obtained at three localities (Chocolate-CH, Frey Pedro-FP, and Cerro-CE; Figs. 2 and 4).

North and east in Olancho Department (Fig. 4a) we collected the Lower Átima Limestone in the southern flank of Montaña Frey Pedro along the road from San Francisco de la Paz to Gualaco (17 sites were collected at Frey Pedro locality, and 15 sites at Chocolate locality). Montaña Frey Pedro is an antiform with a core of metamorphic rocks of inferred Paleozoic age (Rogers et al., 2007c). The Frey Pedro structures include steeply dipping Cretaceous carbonate and clastic rocks forming NW striking folds (Fig. 4a). The Aptian Lower Átima Formation consists of massive to thickly bedded limestone, including fossiliferous and bioturbated wackestone, peloid-foram packstone, and rudstone beds. Rogers et al. (2007c) reported a thickness of about 250 m for this unit. Monopleura and Toucassia genus and benthic foraminifera identified at the Chocolate Hill locality do not provide age constraints, but the genus Amphitriscoelus (Caprinidae) indicates the rocks are lower Aptian (G. Alencaster, personal communication 2009).

Valle de Ángeles strata south of Montaña Frey Pedro dip steeply in the flanks of a WNW trending syncline, and are cut by mafic to intermediate dikes. Here, Valle de Ángeles consists of red polymictic lithic breccia and conglomerate with limestone, sandstone and andesite clasts, as well as reddish orange, lenticular, 0.5–2 m thick beds of sandstone (channel fill) interbedded with purplish-red (overbank)

mudstone. Some sandstone may have been deposited in high-energy marine environments. Sandstones are moderately well cemented. In sections in the Frey Pedro area, lateral accretion bars suggest that Valle de Ángeles Formation was deposited in a meandering river system. In well-exposed sections, Rogers et al. (2007c) described a decrease in limestone clasts up-section and an increase in volcanic clasts. The sandstones of Valle de Ángeles at Ocote are mostly volcanic-arenites or lithic arkoses rich in volcanic lithics, occasionally tuffaceous. Volcanic sources are evident, as well as hydrothermal alteration at the source. Samples contain non-ondulatory monocrystalline and polycrystalline quartz in addition to volcanic lithics, albite, white mica, and glauconite. Hematite cement predates calcite cement. At the Ocote locality (OC) we collected a sample from a mafic dike for ^{40}Ar-^{30}Ar dating to determine maximum deposition age (sample 060509B). Here we also collected a sandstone sample for detrital zircon geochronology (060609C) and a total of 19 paleomagnetic sites.

Samples from the Lower Átima were also collected north of the town of Manto at the Cerro locality. This locality lays also in the southern flank of Montaña Frey Pedro along strike of the structure containing the Chocolate Hill locality, but about 40 km to the west (CE locality, 13 sites). The CE locality is on the south dipping limb of a NW to SW trending syncline (Fig. 4a). Two samples were collected from volcanic rocks of the Manto Formation for Ar-Ar dating. An andesite (sample 060509E) at a road cut at UTM 16P 567,905 1,651,427 and an additional sample of basalt (sample 060509F) at a quarry near San Antonio at UTM 16P 574,302 1,639,387 about 10 km SE of the Cerro locality (Fig. 4a).

The Valle de Ángeles was sampled at two localities in the Yoro area (Fig. 4b). Folds in the Yoro area have the same general NW trend as the folds in the Agalta range. At locality Marale (MA), Valle de Ángeles directly overlies basement rocks. At the Yorito locality (YO, Fig. 4b) sites were collected on the southwest dipping flank of an upright NW trending anticline about 11 km north of Sulaco, where Valle de Ángeles overlies Átima strata and it is discordantly covered by Cenozoic limestones. Samples at Marale include lithic tuff, with fine-grained lapilli, and litharenite. At MA six sites are from gently north dipping strata overlying basement rocks about 14 km east of Sulaco (Fig. 4b). An andesite clast about 60 cm in diameter was collected for ^{40}Ar-^{39}Ar age dating (061209A). Here the Valle de Ángeles consists of coarse-grained lithic sandstone, conglomerate, and red mudstone. At Yorito sandstones are immature with white mica, volcanic lathwork lithics, and low-grade metasedimentary rocks. Sandstone beds are lenticular, and often contain shale intraclasts.

The last locality in the Valle de Ángeles was sampled in southeast Honduras, along the Moroceli-Denli highway (Fig. 4c). At the Moroceli locality, Valle de Ángeles dips gently to the southeast; at this locality Valle strata consist of reddish orange lenticular sandstone beds about 0.5 to 1.5 m in thickness, and thick mudstone intervals about 5 m thick. They form finning upward cycles with common conglomerates, forming channel fill, that include volcanic rock clasts. A fragment of basalt was collected for ^{40}Ar-^{39}Ar age dating (061209B). Valle de Ángeles crops out along a NNW trending fold that is discordantly overlain by Padre Miguel ignimbrites. Jurassic Agua Fría strata, as well as Átima limestones, crop out along the core of this structure. A sample of sandstone in the Agua Fría Formation was collected for detrital zircon geochronology.

Paleomagnetic analyses consisted of progressive thermal and alternating field (AF) demagnetization. Most analyses of the OC samples were conducted at the paleomagnetic laboratory of the University of New Mexico, using a “2G” superconducting cryogenic magnetometer. The rest of the Valle de Ángeles samples were analyzed at the paleomagnetic laboratory of the Centro de Geociencias, Juriquilla, using a JR5 spinner magnetometer. Samples of the Átima limestones were analyzed at the paleomagnetic laboratory Fort Hoofddijk of Utrecht University, once again using a 2G superconducting magnetometer, in part using an automated demagnetization setup (Mullender et al., 2016). Orthogonal demagnetization diagrams were used to determine the vector composition of the natural remanent magnetization (NRM). Principal component analysis (Kirschvink, 1980) was used to calculate the direction of each isolated component. We further used a combination of Fisher statistics and the methods described in Deenen et al. (2011). When necessary, we combined line-fits and poles to great circles using the paleomagnetic interpretation portal on www.paleomagnetism.org (Koymans et al., 2016). The portal incorporates McFadden and McElhinny (1990) for great-circle and line-fit data, and the fold test of Tauxe and Watson (1994). We also used the fold test of Tauxe (2010).

Selected specimens were used for isothermal remanence (IRM) acquisition experiments in order to characterize magnetic carriers. For this we used a pulse magnetizer with a maximum induction of 1.9 T. We determined thermomagnetic curves for a small collection of limestone samples. The curves were measured in air with a Curie balance.

To determine the maximum age of deposition, and also to gain insights into the nature of the rocks eroded during deposition of this unit, clasts in the Valle Angeles were dated by ^{40}Ar/^{39}Ar whole rock methods with conventional oven step-heating. The samples are volcanic rocks of intermediate composition including clasts, a dike that intrudes the Valle Ángeles at the Ocote locality, as well as volcanic rocks of the Manto Formation collected in the Olancho area (Fig. 4a). Because these are whole rock analysis, we crush and sieved to a relatively coarse grain size for the purposes of radiation safety, handling under vacuum, and avoidance of ^{39}Ar recoil artifacts. However, crushing was to a size below that of any phenocrysts even though these are rare. The crushed materials were washed in acetone several times and rinsed with distilled water. Finally, fresh inclusion-free grains were handpicked under the binocular microscope. Analytical methods are explained in Molina Garza et al. (2012).

Two medium- to fine-grained sandstones samples were collected for detrital zircon analysis. One sample was collected in the Valle Angeles Formation (060609C), and another from Jurassic sandstones mapped as Agua Fría Formation (061309A). Sample preparation included crushing, sieving, Frantz magnetic separation, and Wilfley density separation. A grain mount, including grains of all sizes and forms present, of about 120 zircons per sample was made by hand picking with a binocular microscope zircons from the heavy mineral separate. An epoxy mount of the grains was polished in order to expose the zircon walls; every sample was photographed to evaluate the external structure (shape, roundness, color). Cathodoluminescence images were inspected to obtain details of the interior structure (zonation, inherited cores, inclusions). We analyzed cores and rims of the zircon grains by laser ablation inductively coupled mass spectrometry (LAICP-MS) with a laser beam spot of 23 μm on a target fluence of 6 J/cm. The maximum depositional age was estimated using a weighted mean of the youngest zircon cluster, following the method of Dickinson and Gehrels (2009). All the analyses were made at the Laboratorio de Estudios Isotópicos (LEI) of the Centro de Geociencias-UNAM.

3. Results

3.1. Rock magnetism

In the redbeds of the Valle de Ángeles the IRM acquisition curves indicate the presence of low coercivity and high coercivity minerals, but the signal is dominated by the high coercivity minerals. The low coercivity phase is interpreted as coarse-grained magnetite from steep increase in remanence below about 100 mT. The curves do not reach saturation at 1.9 T, a signal that is interpreted to reside in hematite. A small number of thermomagnetic curves in Átima samples show a pronounced Hopkinson peak, which is characteristic of fine-grained (SD to PSD) magnetite. Despite a weak signal, there is no evidence of magnetic sulfides in the thermomagnetic curves of carbonate rocks.

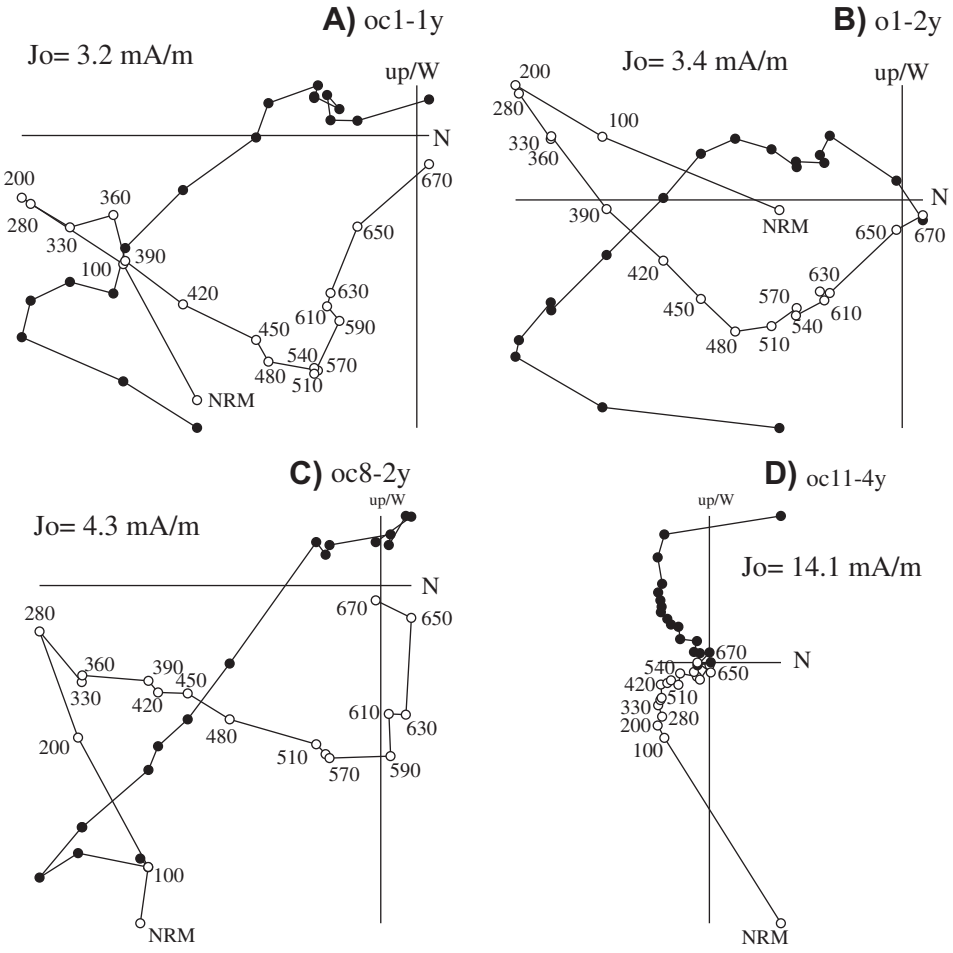

Fig. 5. Orthogonal demagnetization diagrams (Zijderveld, 1967) for samples of the Ocote locality, Valle de Ángeles Formation. Closed (open) symbols are projections in the horizontal (vertical) planes.

3.2. Paleomagnetism

3.2.1. Valle de Ángeles

Samples of the El Ocote (OC) locality are characterized by multicomponent remanent magnetizations. The natural remanent magnetization (NRM) is of moderately high intensities, ranging from about 20 to 200 mA/m. We interpret the demagnetization diagrams to indicate the presence of three magnetization components with partially overlapping laboratory unblocking temperature spectra (Fig. 5). A low-stability component, in in-situ coordinates, is generally north directed and of positive inclinations ranging between about 25° and 55°; it is removed after heating to about 280 °C. An intermediate laboratory unblocking temperature component is removed between about 300° to 500 °C. This component of the NRM is south to southeast directed and of moderate negative inclination (in-situ). The highest temperature component unblocks at temperatures between 590 and 680 °C. Overlapping unblocking temperatures may partially mask the direction of the component of high stability that we interpret as the Characteristic Remanent Magnetization (ChRM). For example, of the four examples in Fig. 5 the high temperature component is only fully isolated in specimen oc8-2y (Fig. 5c); most sites required the combination of stable end-points (SEP) and remagnetization circles to calculate the site mean. The high temperature component is of uniform polarity as indicated by positive inclination and its west-directed declination (in-situ). Site mean directions and statistical parameters are listed in Table 1. Directions used for the calculation of every site are provided in Supplementary Material 1.

Demagnetization diagrams for samples from the Marale locality show a simpler demagnetization behavior than El Ocote samples (Fig. 6). The NRM is also of moderate intensity, of the order of 0.2 to about 35 mA/m. The demagnetization diagrams are interpreted to indicate the presence of two magnetization components with partially overlapping unblocking temperature spectra. A low stability component of the NRM is north directed and of positive inclination, as at Ocote; it unblocks completely after heating to about 350 °C, and makes about 70 to 80% of the NRM. An intermediate to high laboratory unblocking temperature component, defined by linear trajectories to the origin, is southeast directed and of moderately shallow negative inclination in in-situ coordinates. The intermediate to high unblocking temperature component is of distributed laboratory unblocking temperatures between about 400 and 630 °C, and it is isolated in very few samples with lines to the origin; thus site means and overall mean required using great circles and stable directions. Site mean directions are listed in Table 1.

Samples from the nearby Yorito locality show complex behavior during demagnetization, and the NRM is multicomponent (Fig. 6). The first component removed is a positive inclination magnetization of variable north to east directed declinations. Heating to 200 °C is generally sufficient to remove this component. The unblocking temperature spectra of this low stability component overlaps, however, with an intermediate unblocking temperature component, which is south to southwest directed and of moderately shallow inclination (Fig. 6d and f). This magnetization component is isolated at temperatures between 300 and 650 °C. A different behavior is observed in samples from sites yo1, yo2, and yo6 where the magnetization of moderate to high laboratory unblocking temperature is WNW directed and of positive inclination. The magnetization in sites yo1 and yo2 is overprinted by a randomly oriented and high magnitude magnetization of low stability (Fig. 6e). Site mean directions are listed in Table 1.

Finally, the samples collected in the Moroceli locality have

Table 1
Paleomagnetic data (site means) and statistical parameters for sites collected in the Valle de Ángeles Formation, central Honduras. Abbreviations are: stk, dip = bedding attitude as strike and dip; Dec = dclination; Inc = inclination; k(K) and a95(A95) are the statistical parameters of the Fisherian distribution; n(N) is the number of samples used for the calculation of the site (Locality) mean. DDx and Dix are the confidence limits for the Deenen et al. (2011) method. An asterisk (*) is used to indicate sites excluded from final calculations.

	Overprint (interm. comp.)			ChRM (hi T comp.)											
	stk,dip	Dec (°)	Inc (°)	k, α95, n	Dec (°)	Inc (°)	k/K	α95/A95	N/n	ΔDx	ΔIx	Tilt Corrected		(k, α95)	ΔDx	ΔIx
Valle de Ángeles Ocote UTM 592121-1632970																
oc1	258, 81	148.5	−26.5	165.7, 4.3,8	207.4	54.7	16.4	15.4	7			325.6	36.9			
oc2*	264, 81	129.7	−43.2	47.6, 8.1, 8	309.7	34.8	159.4	10.4	5			310.6	−33.2			
oc3*	275, 81	124.2	−11.3	51.7, 7.8, 8	245.3	47.1	6.9	51.1	3			323.6	26.6			
oc4*	264,77	175	−21.1	13.7,25.8, 4	253.7	59.8	10.9	29.2	4			320.7	25.7			
oc5	264,77	138.8	−8.3	50.2, 7.9, 8												
oc6	264,77	146.2	−2.7	44.4,10.2, 6	237.0	41.1	23.3	16.2	5			304.0	28.8			
oc7	264,77	138.9	−8.8	106.6, 5.4, 8	257.6	66.4	46.2	10	6			329.7	14.5			
oc8	264,77	139.5	−20.5	181.1, 4.1, 8	250.7	52.2	26.4	11.8	8			315.1	18.4			
oc9	264,77	153.1	−13.8	102.9, 6.6, 6	239.2	62.9	14	21.6	5			327.4	22.7			
oc10*	264,77				276.8	37.7	9.4	26.3	5			303.5	−1.9			
oc11*	213, 21				265.1	46.0	10.9	29.2	4			273.6	28.1			
oc12	213, 21				264.3	40.1	14.6	18.1	6			271.5	22.5			
oc13	213, 21				286.6	45.8	11.7	23.3	5			290.1	25.3			
oc14	213, 21				258.2	27.3	16	15.6	7			263.1	11.3			
oc15	213, 21				291.5	32.6	17.1	19	5			292.9	11.9			
oc16	123, 38				282.8	51.8	12.4	22.6	5			254.7	29.2			
oc17	107, 43				283.3	28.3	17.3	12.7	9			261.8	13.9			
oc18	157, 32				297.2	38.1	32	8.7	10			285.7	14.9			
oc19	–				–	–	–	–	–			–	–			
Mean OC	In situ	143.9	−17.8 (N = 9, 11.9, 19.6)	All sites	264.9	46.5	17.3	9.1	16/19			296.8	22.4	(10.2,12.2)		
		128.0	45.0	Selected	270.2	44.7	22.0	9.5	12/19	11.16	12.57	308.1	21.5	(18.0, 10.5)	9.94	17.54
				All samples	271.0	42.2	10.0	5.4	*76*	5.96	7.18	310.2	22.7	(16.8, 4.3)	4.35	7.56
				Maxk 40% Sites	290.0	40.0	26.0	8.7	12	9.63	12.24					
				Maxk 40% Samples	292.2	39.3	13.9	4.6	76	5.02	6.49					
Valle de Ángeles Moroceli UTM 523649 - 1556850																
mo1	49, 28				293.0	27.9	223.6	4	7			280.2	51.8			
mo2	48, 18				300.1	29.5	119.3	5.1	8			295.2	46.4			
mo3	48, 18				300.0	25.3	117	8.5	4			295.8	42.2			
mo4	36, 28				285.4	18.8	169	4.7	7			278.2	44.5			
mo5	22, 20				287.2	28.3	408.8	3.3	6			285.7	48.2			
mo6	22, 20				299.2	32.6	71.5	7.2	7			302	52.4			
mo7	22, 20				298.8	21.5	80.6	6.8	7			300.4	41.3			
mo8	22, 20				290.2	24.5	66.7	7.4	7			289.7	44.4			
mo9	180, 26				299.5	40.6	229.3	4	7			293	17.2			
mo10	180, 26				338.3	29.9	176.2	4.6	7			327.8	17.9			
mo11	180, 26				307.9	43.3	34.7	10.4	7			298.7	21.4			
mo12	92, 25				301.6	33.5	190.6	4.4	7			282.9	42.4			
mo13	63, 13				293.8	27.9	59.9	7.9	7			288.2	37.6			
mo14	80, 16				297.4	27	61.5	8.6	6			289.2	35.8			
mo15	80, 16				289.1	29.7	96.7	7.8	5			279.5	36.3			
Mean MO				All sites	298.4	29.8	38.1	6.3	15/15			311.1	24.8	(21.4, 8.5)		
				All samples	298.1	29.9	33.0	2.5	97	2.6	4.1	314.1	25.6	(28.7, 2.8)	2.8	4.7
				Max k 20%	296.0	33.8	57.5	5.1	15							
Valle de Ángeles Marale UTM 485444 - 1645013																
ma1	270, 29	130.7	−44.4	39.7,13.1, 7												
ma2	272, 28															
ma3	254.5, 30.5	116.8	−47.7	34.1,13.0, 8												
ma4	212, 40	115.1	−56.6	138.3, 5.6, 7												

(*continued on next page*)

Table 1 (*continued*)

		Overprint (interm. comp.)		ChRM (hi T comp.)											
	stk,dip	Dec (°)	Inc (°)	k, α95, n	Dec (°)	Inc (°)	k/K	α95/A95	N/n	ΔDx	ΔIx	Tilt Corrected		(k, α95)	ΔDx	ΔIx
ma5	222, 36	100.9	− 52.3	141.4,12.6, 5												
ma6	222, 36	102.4	− 44.0	70.0,33.4, 4												
Mean MA	in-situ	113.4	− 49.5	N = 5, 69.2, 9.3												
Mean tc	Tilt Corrected	118.8	− 37.9													
Valle de Ángeles Yoro UTM 470019 - 1660725																
yo1	118, 28				303.8	33.7	15.9	32.1	3			285.3		32.0		
yo2	118, 28				320.2	48.8	17.6	16.4	6			289.9		48.4		
yo4*	10, 40	187.3	− 23.8	4, 7.1, 37.1	208.2	− 13.3	21.4	16.9	5			212.4		1.1		
yo5*	10, 40	169.4	− 30.6	6, 8.8, 23.9	206.6	− 27.9	16.6	15.4	7			220.3		− 11.3		
yo6*	80, 25	206.0	− 14.2	4, 4, 53.1	238.2	31.3	30.3	14.1	5			227.4		19.7		
		181.7	− 25.5	3, 18.9, 29.2	290.1	43.6	5.6	57.9	3			266.2		38.5	(53.1, 6.9)	
	tc	204.7	− 29.9	52.7, 17.2												
				mo + ma + oc + yo is max k 40%	289.7	39	8.8	15.7	19			290.2		32.7	(10.3, 11.6)	
					290.1	37.7	7.2	22.7								
Mean reverse ovpt		143.5	− 31.6	(17, 13.4, 7.6)												

univectorial magnetizations of high coercivity that are west-northwest directed, and are of moderate inclinations ranging between about 20° and 40° (Fig. 6g). The characteristic magnetization in these sites is of distributed unblocking temperatures, with 80% of the remanence removed after heating to 580 °C. Occasionally there is a north-directed component superimposed on the northwest directed magnetization (Fig. 6h), but it is easily removed upon heating to 200 °C.

The WNW to WSW directed component of moderate to high laboratory unblocking temperature was interpreted as the ChRM of the Valle de Ángeles Formation, and was observed at Ocote, Moroceli and Yoro. The SE directed magnetization of intermediate unblocking temperature observed at Marale sites is considered equivalent to the intermediate temperature magnetization observed in the Ocote sites. We did consider the possibility that the magnetization recorded at Marale is a reverse polarity equivalent of the ChRM, but eventually abandoned this interpretation. The more easterly direction, compared to the southeast overprint at Ocote probably reflects unremoved north-directed overprints as suggested by curved trajectories in demagnetization diagrams (Fig. 6a and b). The isolated sample directions were combined to calculate site means, which are well defined with generally moderate within-site dispersion; the dispersion parameter k varies between about 10 and 46 at Ocote and Yoro, where multicomponent behavior is observed. Better clustering is observed in the Moroceli and Marale sites (k varies from about 40 to about 250). The component of intermediate unblocking temperature of the NRM is well defined at the Marale sites, as well as 9 sites at Ocote and 3 at Yorito. Scatter plots of site means for the Ocote and Moroceli localities are shown in Figs. 7 and 8.

The ChRM is represented by a sufficiently large data set only at Ocote and Moroceli, we thus calculated locality means for these two sets for final paleomagnetic interpretations. OC sites yield a locality mean (in-situ) of D = 270.2° and I = 44.7° (N = 12 sites, α95 = 9.5°, k = 22.0; Table 1), which excludes and outlier and sites with k < 15 and α95 > 25° (Van der Voo, 1990). Correcting for tilt reduces k marginally, from 22 to 18. Using the Deenen et al. (2011) approach, we calculate an in-situ sample mean is of D = 271.0° and I = 42.2° (n = 76 samples; A95 = 5.4°, K = 10, ΔDx = 5.96°, ΔIx = 7.18°). The fold test of McFadden (1990) indicates a maximum k (26.0) at 40% unfolding, but it is not statistically significant. A bootstrap fold test (Tauxe, 2010) indicates a maximum eigenvalue τ1 between 18 and 63% unfolding (Fig. 7). A similar result was obtained with the Moroceli data, where the in situ mean is of D = 298.4° and I = 29.8° (for N = 15 sites; α95 = 6.3°, k = 38.1), or D = 298.1° and I = 29.9° for 97 samples (A95 = 2.5°, K = 33, ΔDx = 2.6°, ΔIx = 4.1°). Tilt correction decreases the k value from 38.1 to 21.4. The maximum value of k is obtained at 20% unfolding (57.5), and for sample directions the bootstrap fold test indicates a maximum τ1 between − 50 and 60% unfolding (Fig. 8).

The reversed polarity overprint, defined by a total of 17 sites in the Valle de Ángeles has an overall mean of D = 143.5° and I = − 31.6° (α95 = 7.6°, k = 13.4). The relatively high dispersion of site mean directions for the reverse polarity magnetization may reflect variable underprinting or overprinting, because of unremoved (lower unblocking temperature) north-directed or (higher unblocking temperature) west-directed components present in these rocks. At Ocote the post-folding age for this magnetization is more evident, because the tilt-corrected directions are southeast directed and of positive inclination (Fig. 7). A formal fold test is presented below.

3.2.2. Átima

Samples of the Lower and Upper Átima Limestone respond well to demagnetization, but the NRM is multicomponent and overlapping coercivity or unblocking temperatures is a common behavior. At the Cerro locality AF demagnetization defines a north-directed magnetization of low (Fig. 9a) to moderately high (Fig. 9b) coercivity, revealing a west-directed positive inclination component. Thermal

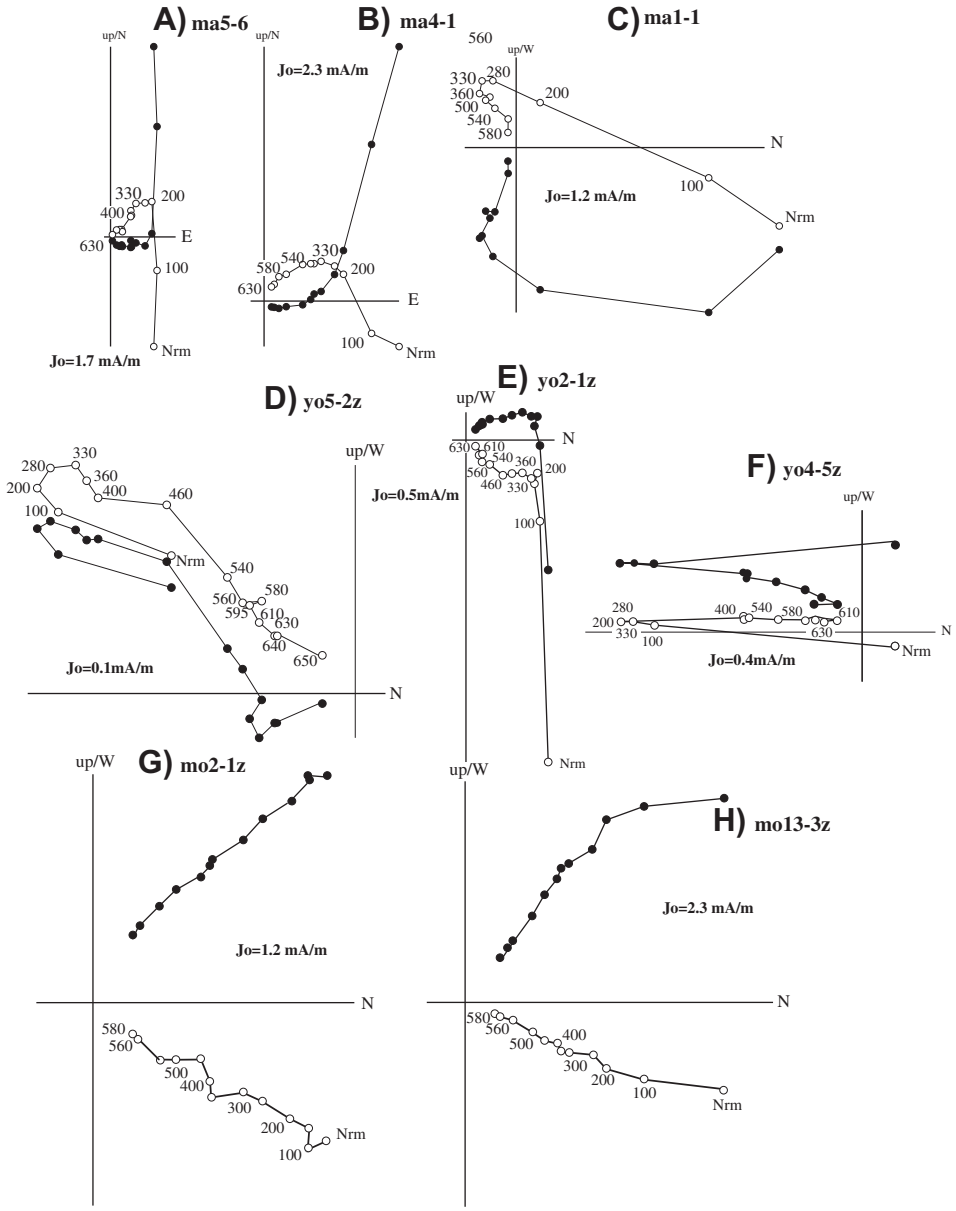

Fig. 6. Orthogonal demagnetization diagrams for samples of the Marale (a-c), Yorito (d-f) and Moroceli ((g-h) localities, Valle de Ángeles Formation. Symbols as in Fig. 5.

demagnetization, however, suggests that AF fails in most cases to reveal the true multicomponent behavior. The WNW to WSW component of positive inclination making a small component of the NRM (Fig. 9c) is often ill resolved. A third component of intermediate unblocking temperature is clearly evident in samples from a handful of sites. This component is southeast-directed, unblocking between about 270 and 390 °C, and its removal reveals the west directed magnetization observed at other sites at still-higher temperatures (always of < 570 °C; Fig. 9d). In some cases, the southeast directed component dominates the NRM in samples AF demagnetized (Fig. 9e and f).

Similarly complex multicomponent behavior is observed at other sampling localities. Samples from Chocolate Hill have a low unblocking temperature magnetization (maximum unblocking temperature of < 200 °C) that is north directed and of positive inclination, and a moderate unblocking temperature component (270 to 390 °C) that is southeast-directed and of negative inclination (Fig. 10a). AF demagnetization may define this component as the dominant remanence with coercivities between about 25 and 90 mT (Fig. 10d). AF, however, often fails to reveal the SE directed component (Fig. 10b), whereas in other cases the presence of this component is evident from the demagnetization trajectories (Fig. 10c). There is no hint at Chocolate Hill of the west-directed magnetization observed at Cerro.

At FP thermal demagnetization is most effective isolating the different components of the NRM. A north-directed magnetization of low coercivity overprints a west-directed magnetization of positive inclination (Fig. 10g). AF demagnetization suggests a near-univectorial behavior (Fig. 10f), but both the north directed and the west directed magnetizations are removed simultaneously resulting in curved demagnetization diagrams directed to the origin. In some examples three components are clearly isolated (Fig. 10e). A north-directed low unblocking temperature remanence is removed first, a west-directed moderate positive inclination component is removed between about 210 and 360 °C, and the highest temperature component is the southeast-directed component of negative inclination (maximum unblocking temperature of 510 °C, Fig. 10e).

As in the Valle de Ángeles, the west directed magnetization of positive inclination in the Átima Limestone is interpreted as the ChRM, and the SE directed negative inclination component is interpreted as a younger overprint. At the FP locality, the calculation of site and locality means was first approached using the apparently linear segments of

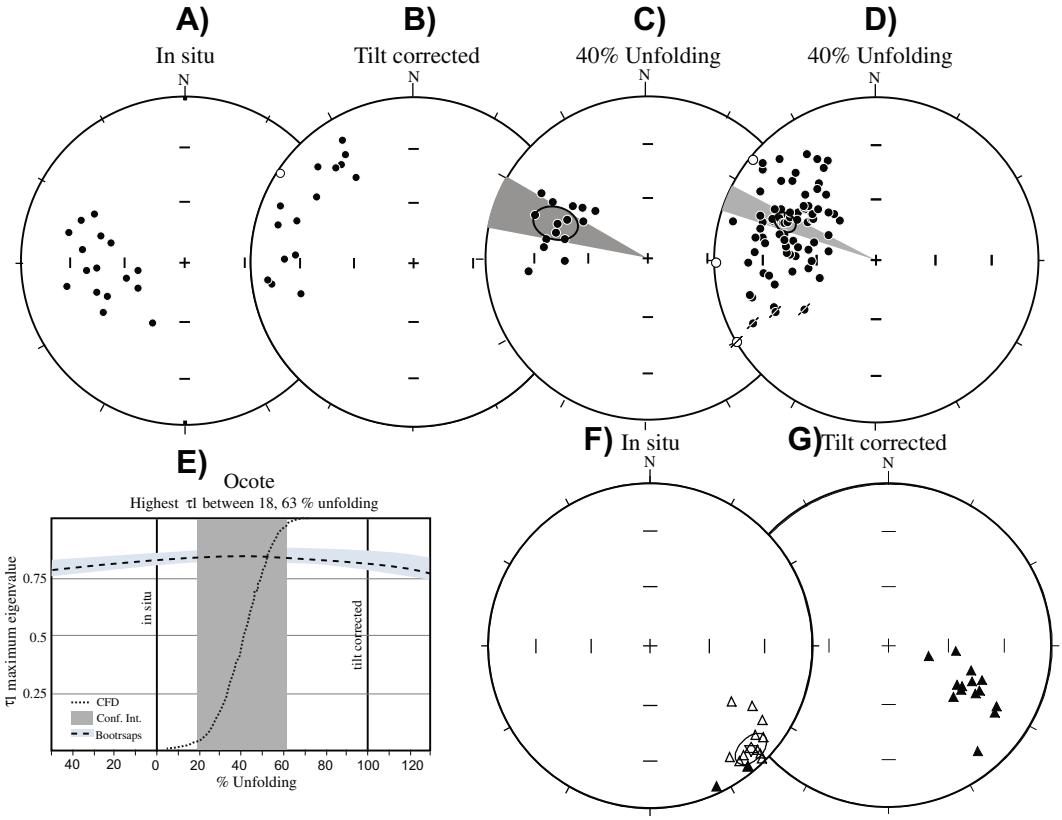

Fig. 7. Stereographic projections of site means (a, b and c) in in-situ, tilt-corrected and 40% unfolding for the ChRM. (d) Fold test after Tauxe (2010) for the ChRM. (e-f) In-situ and tilt corrected site means for the reverse polarity overprint. Ocote locality, Valle de Ángeles Formation. Closed (open) symbols are projections in the lower (upper) hemisphere.

demagnetization diagrams and Fisher's statistics. Within-site dispersion is somewhat variable, with the precision parameter k varying between about 10 and about 180. Site means, however, are well determined. The overall in situ FP mean (Table 2) is of Dec = 300.5° and Inc = 46.5° (N = 17 sites, α95 = 6.4°, k = 32.0), but concerned by unremoved overprints in samples AF demagnetized we calculated a mean based solely in thermally demagnetized samples. For this we used a sample average yielding a mean of Dec = 292.7° and Inc = 46.5° (n = 16 samples, α95 = 9.7°, k = 15.5). Although the difference is small, demagnetization diagrams suggest that thermal demagnetization provides a better estimate of the locality mean because of the overlapping coercivities of the north-directed and west-directed components. A calculation based on a larger dataset that includes stable endpoint directions from thermal demagnetization and great circles defined by AF (32/44, respectively) yields a mean of Dec = 282.1° and Inc = 42.0° (in situ, α95 = 3.6°, k = 17.2), which is the preferred estimate of the ChRM (Fig. 11a). The sites at the FP locality dip near uniformly to the NE in the southern limb of a NW trending syncline cored by strata of the Tayaco Formation. The tilt-corrected site mean direction is of Dec = 347.6° and Inc = 36.5° (α95 = 8.1°, k = 20.4); the precision parameter for the site means decreases with the correction from a high of 32.0 to 20.4. The tilt-corrected mean direction calculated using all

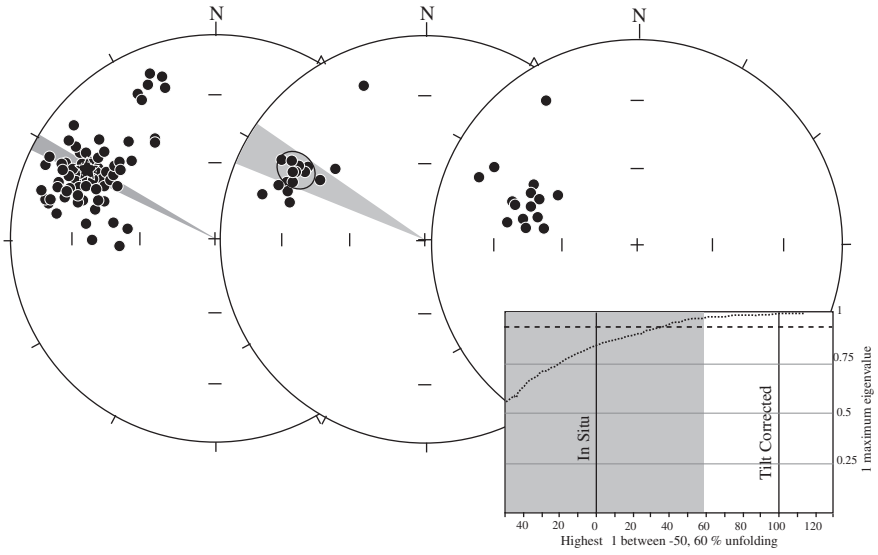

Fig. 8. Stereographic projections of samples (a) and site means (b and c) in in-situ, coordinates for the ChRM. (d) Fold test after Tauxe (2010) for the ChRM. Moroceli locality, Valle de Ángeles Formation. Symbols as in Fig. 7.

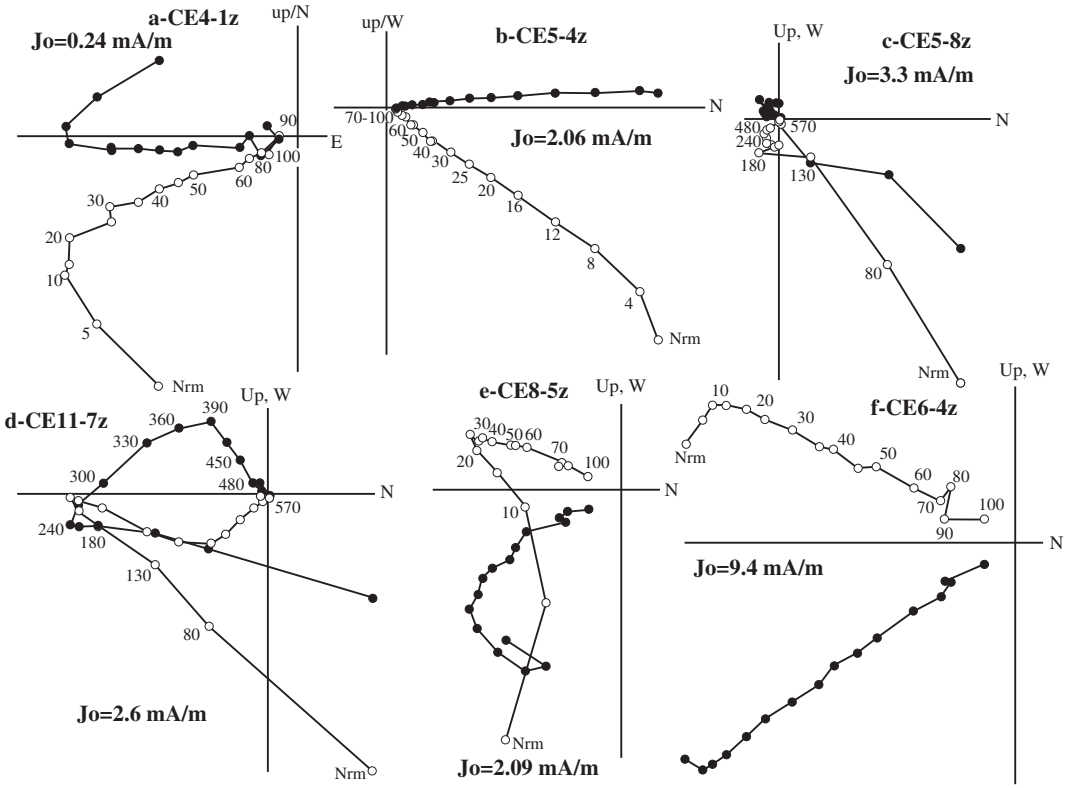

Fig. 9. Orthogonal demagnetization diagrams for samples of the Átima limestone at the Cerro Locality. Symbols as in Fig. 5.

individual directions is of Dec = 335.8° and Inc = 47.4° (A95 = 3.6°, K = 19.2, ΔDx = 3.7°, ΔIx = 5.1°).

At the CH locality a reverse polarity magnetization is well-defined in 7 sites with an in-situ mean of Dec = 143.5° and Inc = − 33.6° (α95 = 6.0°, k = 103.9), which is similar to the SE directed component observed in the Valle de Ángeles Formation. The west-directed magnetization is absent at this Chocolate Hill. At the CE locality the reverse polarity magnetization is observed at nine sites with a mean of Dec = 153.3° and Inc = − 16.0° (α95 = 5.8°, k = 80.4). The west directed magnetization is only present in a few sites at Cerro, we thus determined the locality mean combining the vector directions from 26 samples, all of normal polarity (D = 244.0° ± 8.4 and

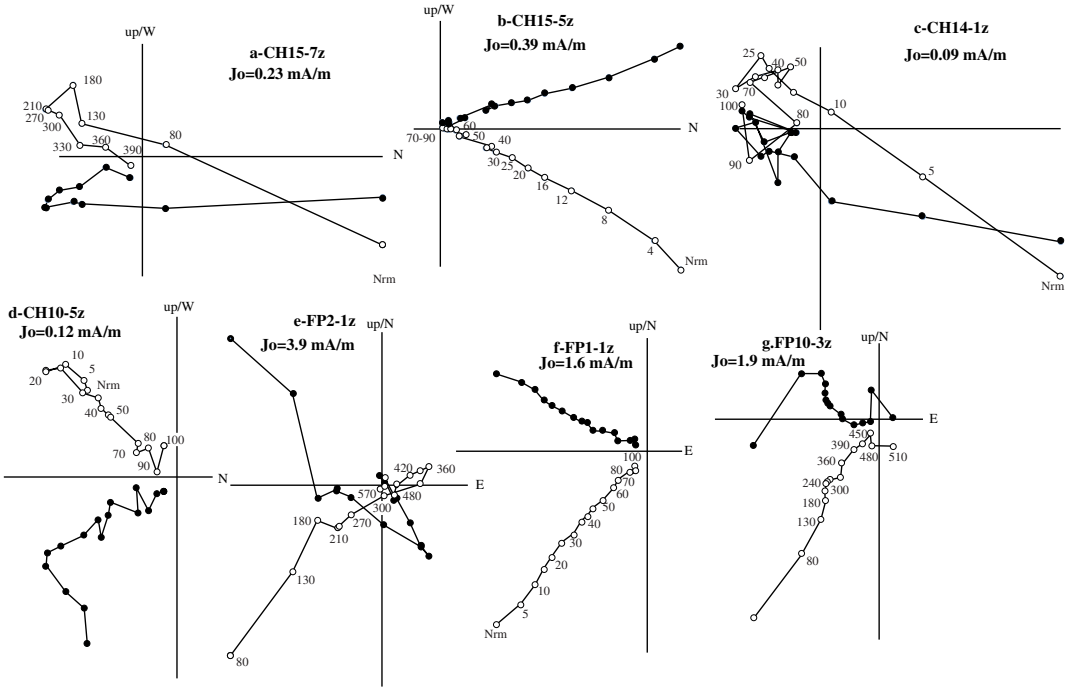

Fig. 10. Orthogonal demagnetization diagrams for samples of the Chocolate (a–c) and Frey Pedro (d–g) localities, Átima Limestone. Symbols as in Fig. 5.

Table 2
Paleomagnetic data (site means) and statistical parameters for sites collected in the Valle de Ángeles Formation, central Honduras. Abbreviations are: stk, dip = bedding attitude as strike and dip; Dec = dclination; Inc = inclination; k(K) and a95(A95) are the statistical parameters of the Fisherian distribution; n(N) is the number of samples used for the calculation of the site (Locality) mean. DDx and Dix are the confidence limits for the Deenen et al. (2011) method. An asterisk (*) is used to indicate sites excluded from final calculations.

	Overprint (interm. comp.)			ChRM (hi T comp.)											
	stk,dip	Dec (°)	Inc (°)	k, α95, n	Dec (°)	Inc (°)	k/K	α95/A95	N/n	ΔDx	Δix	Tilt Corrected		(k/K, α95/A95)	ΔDx	Δix
Atima Formation Montaña Frey Pedro UTM 589775 - 1649961																
FP1	321/58				294.8	50.8	19.1	18.0	5			3.0	40.4			
FP2	321/58				318.9	40.2	40.4	10.7	6			359.5	21.5			
FP3	321/58				306.4	45.3	9.6	42.3	3			357.7	31.8			
FP4	294/47				300.5	36.8			2							
FP5	321/58				291.6	52.5	47.0	9.9	6			5.1	42.4			
FP6	347/52				278.3	47.1	110.8	6.4	6			24.0	71.9			
FP7	316/27				305.9	50.9	146.9	5.5	6			338.3	47.9			
FP8	294/37				302.8	57.3	69.5	7.3	7			341.0	38.5			
FP9	312/56				284.4	33.0	17.2	16.6	6			329.5	38.8			
FP10	319/53				284.6	50.6			2							
FP11	304/52				298.1	39.0	74.3	7.8	6			334.1	26.8			
FP12	305/51				279.0	40.3	180.7	4.5	7			328.0	41.8			
FP13	310/47				280.1	47.6	70.4	8.0	6			338.0	48.5			
FP14	320/50				313.4	21.6	62.0	7.7	7			335.0	22.4			
FP15	318/48				326.1	37.4	21.1	13.4	7			351.8	18.9			
FP16	318/48				331.9	45.9	10.8	24.4	5			1.7	20.9			
FP17	295/46				302.2	52.2	59.9	7.9	7			340.0	29.0			
				Sites	300.5	46.5	32.0	6.4	17/17			347.6	36.5	(20.4, 8.1)		
				Thermal demagnetization	292.7	46.5	15.5	9.7	*16*			342.8	41.2	(13.4, 10.5)		
				All (GC + SEP)	282.1	42.0	17.2	3.6	32 + 44	4.0	4.5	335.8	47.4	(19.2, 3.6)	3.7	5.1
Atima Formation Chocolate Hill UTM 590223 - 1646600																
CH5	136/29.5	143.2	− 33.3	14.3, 25.2, 4												
CH7	160/13.5	141.3	− 35.5	2												
CH8	160/13.5	134.0	− 37.6	50.7, 8.6, 7												
CH9	145/16	142.1	− 33.7	1												
CH10	140/17	142.1	− 40.6	139.4, 5.1, 7												
CH11	130/18	145.1	− 28.1	93.9, 12.8, 3												
CH12	115/19	144.9	− 27.6	2												
CH13	105/20	142.7	− 27.5	64.5, 15.5, 3												
CH14	105/26	145.8	− 42.2	67.6, 11.3, 4												
CH15	105/26	150.6	− 35.3	22, 13.2, 7												
MEAN		143.5	− 33.6	103.9, 6.0, 7												
Atima Formation Cerro Locality UTM 568074 - 1653426																
CE2	63/24															
CE3	63/24	162.9	− 6.8	77.0, 25.8, 6	245.9	37.1	16.2	15.4	7			228.3	34.6			
CE4	63/24															
CE6	44/26	134	− 17.8	197.8, 4.3, 7	289.2	39.9	20.0	21.1	4			271.0	61.9			
CE7	108/31	155.2	− 12	24.8, 15.9, 4												
CE8	100/25	152.2	− 21.9	57.2, 9.1, 5												
CE9	65/26	156.6	− 23.2													
CE10	65/26	153.8	− 13.1	20.7, 13.6, 7	247.1	28.9			2			233.2	26.6			
CE11	62/20	158.7	− 13.1	13.3,25.0, 3	234.8	31.7			2			223.7	27.2			
CE12	62/20	152.9	− 14.7	20.6, 19.5, 3	237.0	31.6			2			225.6	27.8			
CE13	62/20	152.2	− 20.7	17.8,16.9, 4	231.8	34.4			2			219,9	28.7			
MEAN		153.3	− 16.0	80.4, 5.8, 9	244.0	33.2	17.7	8.0	26	8.4	12.4	231.8	30.9	(22.1, 7.1)	7.4	11.5

(*continued on next page*)

Table 2 (*continued*)

Cerro, Chocolate, and Ocote reverse polarity												
	In Situ					Tilt Corrected						
	N	Dec	Inc	(k, α95)	ΔDx	ΔIx	Dec	Inc	(k, α95)	ΔDx	ΔIx	
Sites	32	147.0	− 25.0	(22.0, 5.6)			140.0	− 20.5	(7.6, 10.6)			
Samples	176	146.1	− 25.3	(20.1, 3.2)	2.5	4.2	141.6	− 11.8		3.7	7.2	

$I = 33.2^{\circ} \pm 12.2$; K = 17.7, A95 = 8.8°). Maximum k is observed after unfolding (K = 22.1) but the difference is not statistically significant.

We combined the reverse polarity, southeast directed, magnetization from sites in the Valle de Ángeles and Átima limestone for a grand mean of Dec = 146.2°, Inc = − 28.5°; k = 13.1, α95 = 6.8°, N = 37 sites; or Dec = 146.1° and Inc = − 25.3° (ΔDx = 2.5°, ΔIx = 4.2°) n = 176 directions. The collection of reverse polarity sites produces a robust negative fold test with a maximum eigenvalue τ1 between − 11 and 16% unfolding (Fig. 12). A regional tilt test using the west directed ChRM locality means of the Valle de Ángeles and Átima Limestone at OC, MO, FP, and CE yields a robust negative fold test.

3.3. Geochronology

Zircons in the Valle de Ángeles are dominated by subhedral to euhedral grains, and their size range from about 50 to 220 μm in their longest dimension. CL textures show concentric zoning typical of igneous growth. The minority of the grains are subhedral to anhedral with complex textures revealed by CL images, consisting of cores and overgrowths (rims). Zircons in the Agua Fría sandstone are dominated by anhedral and rounded grains. CL textures show abundant homogenous and light grains, or grains with light rims. This are often indicative of a metamorphic source. A sample from the Agua Fría Formation (061309A, n = 93 grains, 5 discordant grains excluded) contains Archean (9%) and Paleoproterozoic (13%) zircons in the range from 2300 to 1650 Ma; a significant Mesoproterozoic (~1300–950 Ma) zircon population (21%) is also present. A dominant Neoproterozoic to Cambrian population with ages of about ~950 to 500 Ma makes 56% of the zircons in the sample, but it is dominated Ediacaran to Cambrian (650 to 500 Ma) zircons (41 grains). The rest of the zircon grains (4) do not conform a population; three are of Early Paleozoic age and one is Carboniferous (Fig. 13; Supplementary Material 2).

A sample from the upper Valle de Ángeles Formation (060609C, n = 107 grains, 2 discordant grains excluded) contains Archean and Paleoproterozoic zircons (2%), a significant Mesoproterozoic (~1600–900 Ma) zircon population (14%), a handful of Neoproterozoic to Cambrian grain ages of about ~900–500 Ma (4%), a Carboniferous to Permian population at ~311–275 Ma (5%), and a dominant Cretaceous population (120 to 85 Ma, with 74% of the analyzed zircons). Within the Cretaceous population, the most frequent ages of zircons are in the Cenomanian (99.6 to 89.3 Ma). Analytical data are included in Supplementary Information 2, and Fig. 13 shows the Tera-Wasser diagrams and density probability plots for the samples analyzed. For this sample, the maximum deposition age is 85.4 Ma.

Results of the ^{40}Ar-^{39}Ar determinations are summarized in Table 3, and analytical data are included in Supplementary Information 3. The sample collected from a dike that cuts the Valle de Ángeles at the Ocote locality does not provide a plateau age, but isochrons calculated with the intermediate temperature steps (604 to 686 °C) and high temperature steps (816 to 1184 °C) yield statistically indistinguishable isochron ages of 61.7 ± 4.6 and 63.0 ± 3.2 Ma. A Paleocene magmatic episode has been recognized in central Honduras (Gose, 1985), with ages of about 60 Ma in the Minas de Oro and San Francisco intrusives. The Chindona batholith crops out north of Montaña Frey Pedro (Fig. 4a); it has been assigned a Paleocene age but no radiometric data are available. The Paleocene date for the dike is considered a reliable age estimate of the age of intrusion because the age and composition of the dike is similar to ages in intrusive rocks reported in the Agalta range and Frey Pedro foldbelt summarized in Rogers et al. (2007a). Combined, the U-Pb detrital zircon data and this date bracket the age of the Valle de Ángeles at the Montaña Frey Pedro foldbelt to between about 85 and 63 Ma. It also constrains the folding in this region to before 63 Ma, in agreement with estimates based on stratigraphic inferences by Rogers et al. (2007c).

One of the basalt samples collected in the Manto Formation (060509E) provides a partial plateau of about 43 ± 1.5 Ma with 9

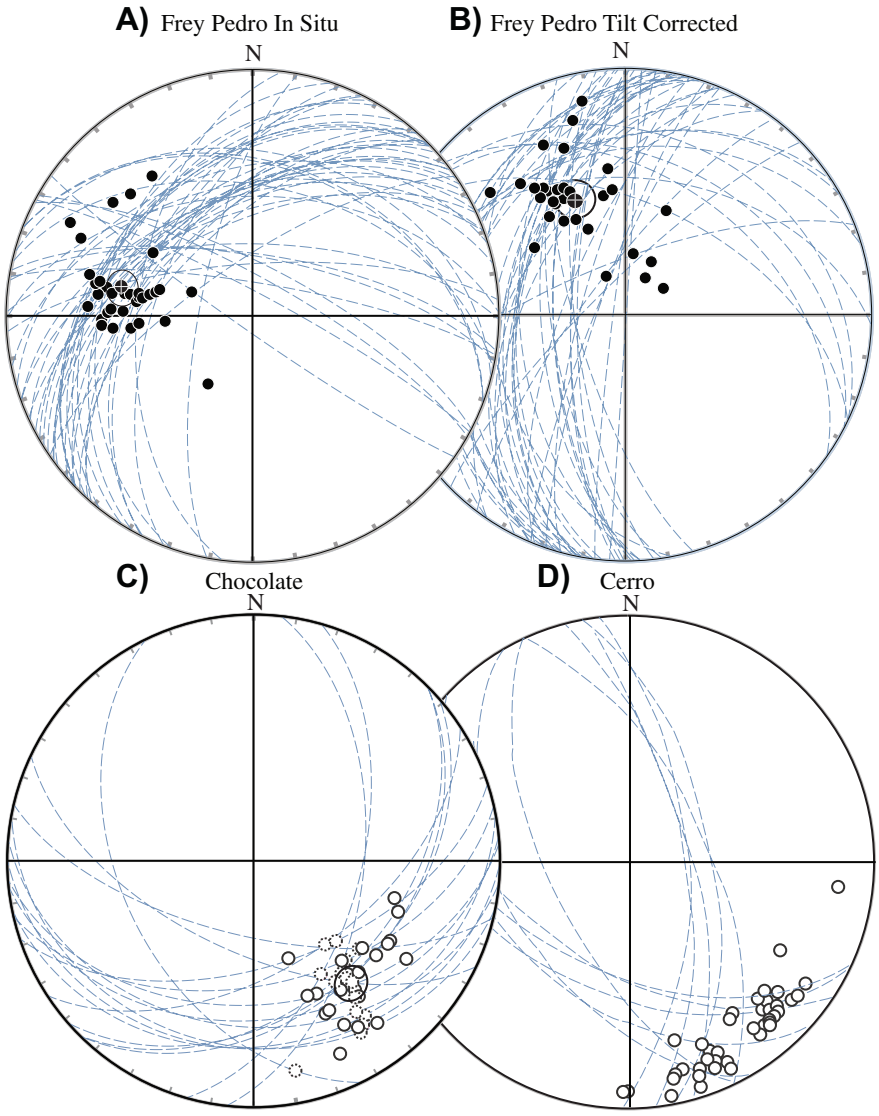

Fig. 11. Stereographic projections of sample stable end-point directions and great circles in-situ (a) and tilt corrected (b) coordinates for the ChRM in the Frey Pedro locality. Stereographic projections of sample stable end-point directions and great circles in-situ for the reverse polarity magnetization at Chocolate (c) and Cerro localities; Átima limestone. Symbols as in Fig. 6.

steps in the range from 506 to 918 °C. The other sample (060509F) does not define a plateau age, but an isochron of 70.8 ± 3.3 Ma was determined. This age is within error of the weighted mean of steps 3 to 7 of 72.4 ± 1.3 Ma. These ages are significantly younger than suggested by the known biostratigraphy. The ages may thus reflect Ar loss or alteration. The two other clasts in the Valle de Ángeles also yield disturbed Ar released spectra. Sample 061209A is a whole rock experiment in basalt that yields an Ar release spectra climbing steadily to ages ranging from 100 to 120 Ma. Sample 061209B provides a partial plateau defined by 6 steps in the range from 459 to 506 °C, with a resulting date of 52.7 ± 1.8 Ma. An isochron was determined with a date of 50.3 ± 2.9, which is the preferred age estimate of this andesite clast. These ages are younger, however, than the age assigned to the top of the Valle de Ángeles Formation based on stratigraphic arguments (Gose and Finch, 1992). We do not know, however, of geologic or other evidence for this inferred age. If the age of the andesite clast is reliable, it would indicate that the Valle de Ángeles may be as young as Lower Eocene at the Moroceli locality. However, because none of the clasts dated yielded well-defined plateaus and some the isochron ages are not compatible with the known stratigraphy we do not consider the Lower Eocene age reliable. We do note, however, that the ages around 50 Ma observed in the clasts may reflect a regional tectono-thermal event affecting the region.

4. Discussion

4.1. Paleomagnetic constraints on the Late Cretaceous to Paleogene motion of the Chortis Block

The multicomponent behavior of the NRM and its apparently synfolding age make interpretation of the ChRM not straightforward. Demagnetization experiments show that, more often than not, there are three stable components to the NRM (Figs. 5–10). The north-directed and moderate inclination magnetization is interpreted as a magnetization of recent origin (possibly viscous). We will not discuss this component further, other that it often contaminates the other observed components; this is particularly evident in AF demagnetization experiments. It is also evident that this magnetization resides partly in a magnetically hard phase, but mostly in a magnetically soft phase assumed to be magnetite.

Demagnetization diagrams reported by Gose (1985) include thermal demagnetization up to 400 or 500 °C in Átima and other limestones and up to 600 °C in the Valle de Ángeles and other redbeds, occasionally combining AF (first) and thermal demagnetization after that. A significant magnetization remains after the highest temperature step used in that study. The magnetization of the Átima Limestone and Valle de Ángeles Formation was reported by Gose (1985) as nearly univectorial, or as two components: a west directed ChRM with a north directed but

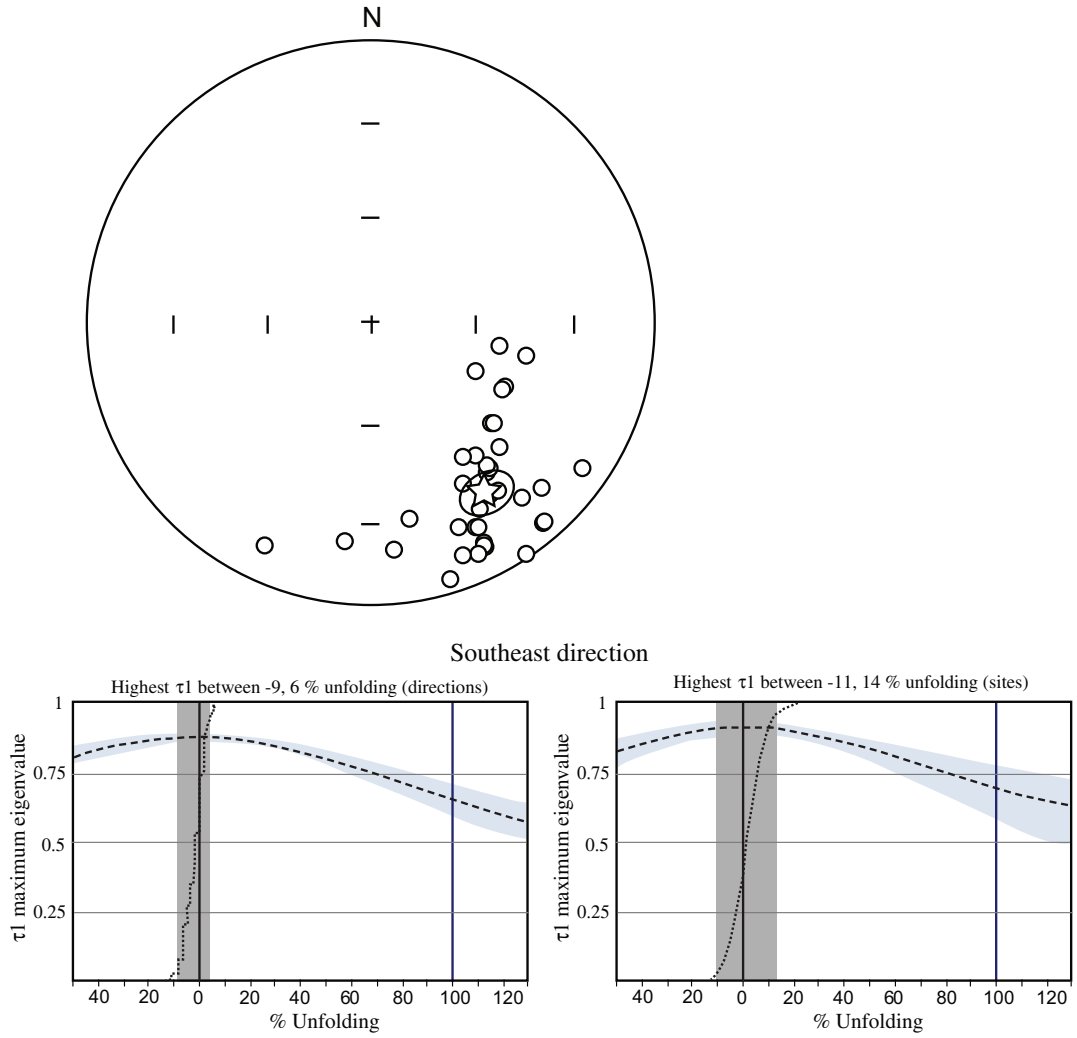

Fig. 12. Stereographic projections of site means in in-situ coordinates (a) for all localities for the reverse polarity southeast directed component. (b) and (c) are the fold tests of sample and site mean directions, respectively.

small overprint. While this behavior was observed at some localities, such as FP and MO, in most of the limestones and redbeds it is evident that detailed thermal demagnetization is required to isolate the vector components defining the NRM. The ChRM is also reported by Gose (1985) to predate Late Cretaceous folding on the basis of a qualitative fold test. Our fold test results conclusively indicate otherwise: the interpreted ChRM post-dates (most of the) folding and is not the primary magnetization. Although the results of Gose (1985) are partially reproduced in this study (Fig. 14), the mean directions reported by this author are likely contaminated or represent composite remanence vectors.

A reverse polarity, southeast directed magnetization of moderately low inclination is recognized as an overprint in 17 of the redbed sites as well as 21 of the limestone sites; it is not present at the Moroceli and Frey Pedro localities. The robust regional negative fold test indicates that this intermediate unblocking temperature magnetization was acquired after folding (Fig. 12). The mean directions of this component from Ocote and Cerro are indistinguishable, but inclinations are higher at Chocolate. The directions observed suggest that this magnetization may record a regional thermal event related to Paleogene or younger magmatism, which may be also responsible for disturbing the ^{40}Ar-^{39}Ar systematics and may explain the young ages in clasts of volcanic rocks included in the Valle de Ángeles. We recognize that SE directions of negative inclination were reported by Gose (1985) for Paleocene intrusions in central Honduras, namely the San Francisco and Minas de Oro plutons (Fig. 14). The mean of four sites reported by Gose (1985) is of D = 126.8° and $I = -15.7°$, despite being determined in only four sites with poorly grouped directions, is comparable to the reverse polarity component observed in our extensive analysis. The intermediate unblocking temperature reversed component is secondary but ancient. It is statistically distinctly different from the Miocene field direction recorded in the ~15 Ma Padre Miguel ignimbrite suite (Dec = 352.0 ± 6.1°, Inc = +16.9 ± 11.3°; n = 26, K = 23.1, A95 = 6.0°, k = 18.7, α95 = 6.7°, Molina Garza et al., 2012). The mean inclination for the reverse polarity overprint component (McFadden and Reid, 1982) is $I = -27.1$ (k = 16.3, α95 = 4.9°), indicating a paleolatitude of 14.4° ± 2.7°N. The age of this remanence is bracketed between about 50 Ma, i.e. the reset ^{40}Ar-^{39}Ar ages that we tentatively link to the remagnetization event, and the age of the Padre Miguel ignimbrites (15 Ma). A tectono-thermal event affecting Chortis at about 50 Ma may reflect the onset of eastward motion recorded in the Cayman Trough.

The ChRM in both the Átima limestones and Valle de Ángeles redbeds is west-northwest directed. A fold test indicates that this magnetization is post- or, more likely, syn-folding. The magnetization is thus secondary but ancient. What we interpret as the most reliable estimates of this component are the early-synfolding site mean directions at Moroceli and Ocote, which are of Dec = 296.0° - Inc = +33.8° (k = 57.5, α95 = 5.1°, N = 15 sites) and Dec = 290.0° - Inc = 40.0° (k = 26, α95 = 8.7°, N = 12 sites), respectively. These compare well

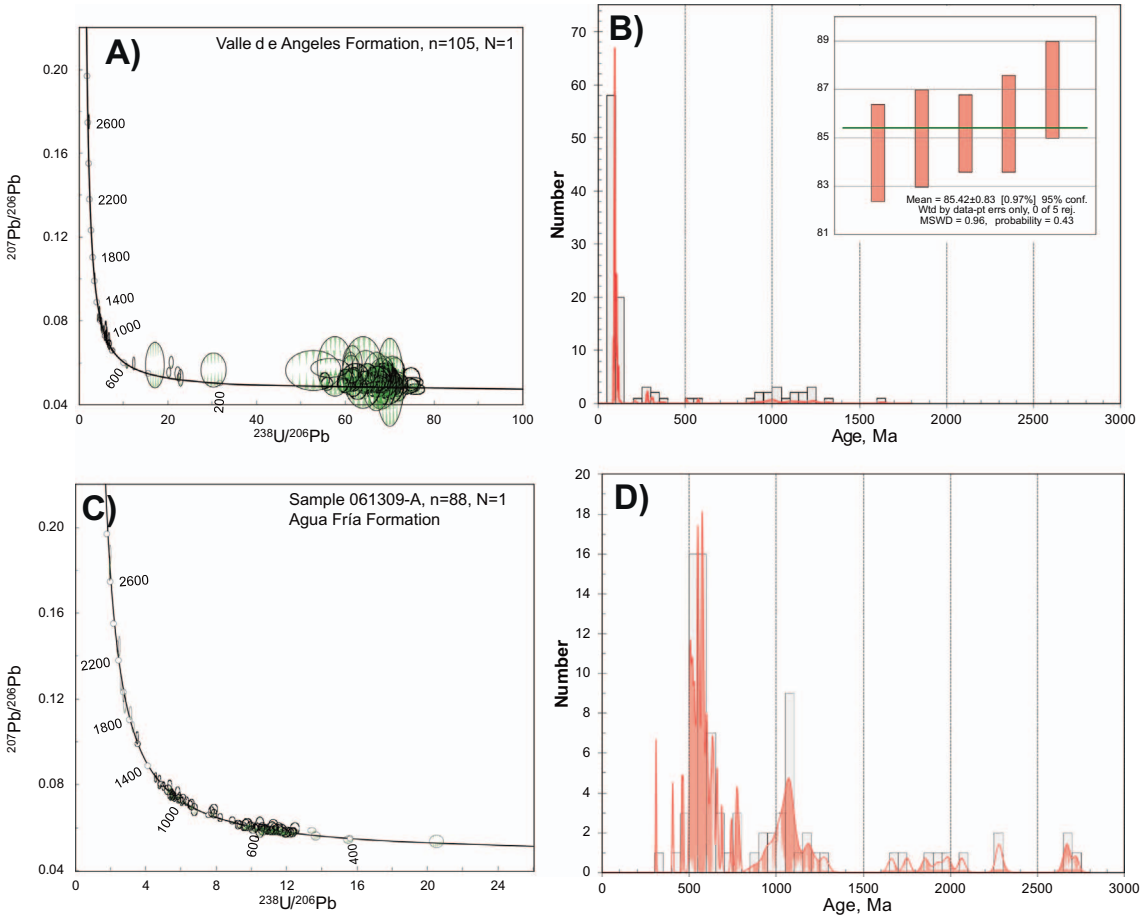

Fig. 13. Detrital zircon geochronology for the Valle de Ángeles (a–b) and Agua Fría Formations (c–d), showing a Tera-Wasserburg diagram and density probability plots with associated hystograms (Zihuatanejo and Mexcala from Talavera-Mendoza et al., 2007; Tehuantepec from Pérez-Gutiérrez et al., 2009). Notice the greater contribution from the Cenomenian-Turonian arc at Valle de Ángeles.

with the mean in situ directions observed at Frey Pedro (282.1°, 42.0°) and Yorito (290.1°, 43.6°). Cerro locality shows, however, a more westerly declination (247.4°, 34.8°). The orientation of major folds and faults in all localities is similar (~300° strike), except at Cerro where fold axis trends nearly east-west, likely associated with structural complexity such as resulting from basement heterogeneity. Local rotation may thus explain the anomalous declination at Cerro. If this interpretation is correct, the reverse polarity overprint is not affected by the change in fold trend because similar directions are observed at Cerro and other localities for this component. The mean inclination for four localities is 39.7° (k = 108.9, α95 = 6.8°) for a paleolatitude of 22.5° ± 3.6°N. The age of the magnetization is bracketed between 84.5 (the maximum deposition age) and Paleocene (~63 Ma, the age of post-folding intrusions).

These results are similar to those reported by Gose (1985), as shown in Fig. 14. The site means reported by this author were combined by age or geographic distribution. It appears that sites that yield SW directed and positive magnetizations are from a single locality. The directions reported by Gose (1985) are also predominantly of normal polarity (29 out of 32 sites.

We calculated rotation (R) and flattening (F) estimates for both the ChRM and the reverse polarity overprint, by comparing the observed

Table 3
Summary of Ar-Ar geochronology.

Sample	Locality	Rock	Mineral	Steps used T/OP	cum39Ar (%)	Spectrum age	Int.2σ	Isochron age	Int.2σ	MSWD
060509B-Dike	Ocote	Basalt	w.r					61.76	4.56	3.267
UTM 872798 150206								Isochron 604–686 °C, 12.33% cum. ^{39}Ar		
								62.98	3.15	2.110
								Isochron 816–1184 °C, 18.66% cum. ^{39}Ar		
060509E- Manto Fm.	Cero	Andesite	w.r.	3 to 7	45.27	72.36	1.35	70.82	3.32	2.392
UTM 567905 1651427				478–603 °C		Weighted mean				
060509F- Manto Fm.	Cerro	Basalt	w.r	4 to 15	54.88	43.43	1.56	41.19	7.22	1.430
UTM 574302 1639387				506–918 °C		Plateau				
061209A-clast	Yorito	Andesite	w.r.	Climbing steadily to ages ranging from 100 to 120 Ma; no partial plateaus.						
UTM 469916 1660632										
061209B-clast	Moroceli	Basalt	w.r	2 to 7	52.67	53.97	1.81	50.23	2.87	1.730
UTM 872798 150206				459–605 °C		Weighted mean				

TCR used as age standard, 28.619 ± 0.034 Ma.
Assumed atmospheric ratio is 298.56 ± 0.31.

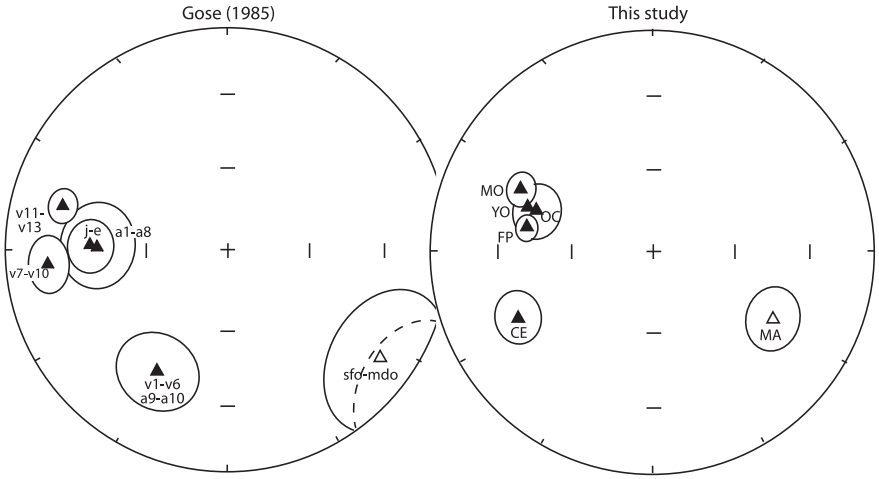

Fig. 14. Summary of paleomagnetic directions observed in Cretaceous strata and Paleocene intrusions in the Chortis block after Gose (1985) and this study. Letters and numbers (v1, a1, etc.) identify sites reported by Gose (1985) averaged geographically or temporally. Paleocene plutons (sfo-mdo) correspond to the San Francisco and Minas de Oro sites of Gose (1985).

direction with the North America craton reference direction. We used as reference pole the 70 Ma estimate of Torsvik et al. (2008) for the WNW directed ChRM, and the ~30 Ma reference direction for the reverse polarity overprint. For the ChRM the calculations of R and ΔR are 49.4 ± 7.5° (Moroceli), 63.2 ± 6.7° (Frey Pedro), 55.3 ± 10.7° (Marale), and 105.3° ± 9.9° (Cerro). They average to about 55.4 ± 5.7°. There is some uncertainty on the age of the characteristic magnetization, as its time of acquisition is bracketed between about 84 and 63 Ma. This, however, does not have a significant effect on the rotation estimate because there is very small apparent polar wander of North America during this time. The average rotation estimate would account to 53.9° if the magnetization was acquired at 60 Ma, or 57.2° if the magnetizations was acquired at about 80 Ma.

The estimates of F for the ChRM range between 1.4 ± 11.5° and 10.2 ± 7.6°; the best estimate of F is 7.7 ± 10.4°, combining data from all localities. For the reverse polarity overprint, again assuming it was acquired at ~30 Ma, estimates of R and F are 26.5 ± 7.7° and 5.3 ± 8.5°, respectively. By inference, a rotation of about 30° occurred between acquisition of the ChRM (assumed at 70 Ma) and acquisition of the reverse polarity overprint (assumed at 30 Ma) with a latitudinal displacement of ~600 ± 800 km. As in the case of the ChRM a difference of 10 million years in the age assigned to the overprint would no bring a significant difference in the estimate of rotation because of the small amount of APWP recorded by North America.

A latitude of 22.7°N is expected for a reference point in coastal Mexico near Acapulco at about 70 Ma using the APWP and plate circuit of Torsvik et al. (2008) (Fig. 15). We notice that this paleolatitude is significantly higher than observed in the Caribbean plate east of the Southern Nicaragua Rise at ODP sites 999 and 1001 (12.74°N, 281.26°E; 15.76°N, 285.09°E, respectively; Fig. 2), which place the present-day Hess escarpment at about 5°N at 70 Ma (Acton et al., 2000). It is unclear, however, if the basalts sampled at these sites average secular variation.

4.2. Implications of provenance data, the Cenomanian-Turonian arc

Fig. 15 shows the Chortis block reconstructed after restoring 55° of counterclockwise rotation relative to NAM. The reconstruction is based on an interpretation of the ChRM to have an age of ~70 Ma. The reconstruction is valid for that age, and places the Frey Pedro locality at a latitude compatible with that of the city of Acapulco. This reconstruction is very similar to what was proposed by Rogers et al. (2007a), which used a prominent magnetic anomaly in aeromagnetic maps from both Honduras and Mexico. In Mexico this anomaly is interpreted as the Arperos-suture between the Guerrero superterrane and mainland Mexico. The reconstruction is supported by stratigraphic ties between the central Chortis terrane and the geology of the Guerrero state area (Guerrero-Morelos platform in the Fig. 15); these were first noted by Rogers et al. (2007a), but are revised here in Fig. 3. The reconstruction is also supported by pre-60 Ma deformation history between Chortis and Mexico during the later stages of the Laramide orogeny evident in the correlation of similar trends in Upper Cretaceous structures in the Frey Pedro area and the Guerrero-Morelos platform noted by Rogers et al. (2007a).

The Xolapa terrane contains a record of post-Laramide deformation in the form of migmatization and ductile deformation. The structural data for the region of coastal Oaxaca is, however, ambiguous. Corona-Chávez et al. (2006) interpreted structural fabrics in the Xolapa Complex to reflect northward compression, while Ratschbacher et al. (1991) interpret the fabrics to reflect N-S extension, and even propose a back-arc setting for the complex. Our model is in agreement with Ratschbacher et al. (1991). A record of N−S extension was proposed by Peña-Alonso et al. (2017) for the late stages of the Laramide orogeny, based on migmatites in the Puerto Escondido area. Fig. 15 shows the principal outcrops of Cretaceous and Paleogene plutons in southern Mexico and Chortis, as well as localities in southern Mexico for which detrital zircon geochronology is available for Upper Cretaceous strata. The localities are Zihuatanejo, Mexcala, and Tehuantepec.

Detrital zircon geochronology of Jurassic Agua Fría strata from the central part of Chortis is consistent with southern Mexico data; the zircon populations in Agua Fría strata are observed in southern Mexico basement terranes, such as the Paleozoic Acatlán Complex of the Mixteca terrane (Talavera-Mendoza et al., 2005). Pan-African and Grenville zircons are dominant in this basement unit of Mexico, and are often observed as recycled zircons in younger strata (e.g., Campos Madrigal et al., 2013; Sánchez-Zavala et al., 2004). The compositional maturity of sandstones in the Tecocoyunca Group of the Tlaxiaco basin in southern Mexico is also similar to Jurassic sandstones in the Denli area of Honduras (R. Rogers, unpublished data). Other similarities between Mesozoic strata in Mexico and central Chortis include the association of continental strata with ash flow tuffs at the base of the Jurassic section, and the presence of ammonite bearing marine strata in the Middle Jurassic. We note also that the transition from continental to marine deposition is recorded by Aptian strata of the Tepemechin and Átima formations in Honduras and by the Atzompa and Zicapa formations in southern Mexico; in both areas deposition of Lower Cretaceous strata occurred in a intra-arc to back-arc setting (Sierra-Rojas et al., 2016; Rogers et al., 2007c).

Our single analysis of detrital zircons from the Valle de Ángeles Formation (displaying grains in the age range between about 100 and 85 Ma) confirms the position of the Chortis block, rotated ~55°, at the southern end of Oaxaquia by explicitly extending the Cenomanian-Turonian (Laramide) arc along the western edge of the greater Oaxaquia block into Chortis (Figs. 1 and 15). Furthermore, by

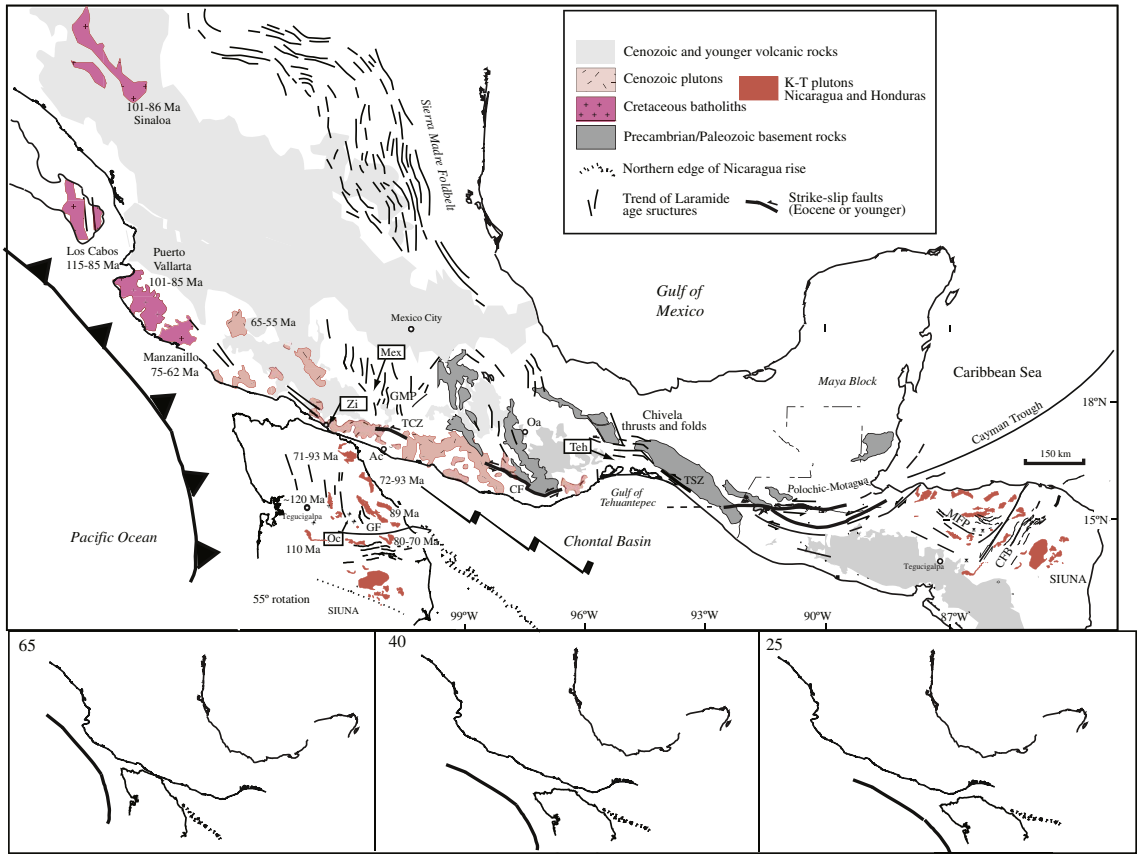

Fig. 15. Reconstruction of the Chortis block after rotation of 55°, with occurrences of Cretaceous-Paleogene magmatism and the principal trends of Laramide-age folding. We include the Paleogene (?) Chivela fold belt of Pérez-Gutiérrez et al., 2009 in the Tehuantepec area. The reconstruction time is estimated for about 65 Ma, and the frames below show the motion of Chortis as it first rotates 30° between about 65 and 40 Ma, and then between about 40 and 25 Ma to close the Chontal basin.

establishing this continuity it suggests that the arc trends offshore to the south into oceanic crust to intersect a transform plate boundary. This boundary is linked, perhaps, to the inferred NW Caribbean arc of Pindell and Kennan (2009). The subduction of the Farallon slab below NAM, however, must have terminated just south of Chortis in the triple junction with the Caribbean plate boundaries. Restoring the Caribbean plate back into its Late Cretaceous position inevitably requires, given that there is no record of major Late Cretaceous to Cenozoic plate-wide extension within the Caribbean plate, that the Central American portion of the plate was much farther to the west than the FAR-NAM trench (as illustrated in Fig. 1). While there may have been a subduction zone along the Western Caribbean plate margin in the Late Cretaceous (Pindell and Kennan, 2009), geological evidence for this remains sparse (unlike the widespread volcanism and deformation associated with the Laramide orogeny). The Cenomanian-Turonian NAM arc has no connection with the Greater Antilles arc, which by 70 Ma had already collided with the Maya Block of Yucatán in the Motagua suture (Pindell and Kennan, 2009; García-Casco et al., 2008).

Fig. 16 shows that Upper Cretaceous units deposited in southern Mexico (e.g., Zihuatanejo, Cutzamala, and Mexcala Formations) and Honduras (Valle de Ángeles) have a significant contribution from the Cenomenian-Turonian arc, which formed over the Laramide slab near its southern termination. These localities, as well as Upper Cretaceous strata in the Tehuantepec area (Pérez-Gutiérrez et al., 2009) show contributions from similar arc (Cretaceous) and basement (Grenvillean) sources. The proportion of Cretaceous arc sources is higher for the Valle de Ángeles, which was deposited closer to the axis of the arc. This is also supported by Valle de Ángeles sandstone composition and the presence of lithic tuffs at Yorito. The relative contribution from basement sources is higher in the Tehuantepec locality, which is far removed from the arc (Fig. 15).

4.3. Regional kinematic and geodynamic implications

In the reconstruction of the Caribbean region of Boschman et al. (2014), the Chortis block was reconstructed westward of its present position between 0 and 50 Ma, based on North America – Caribbean motion as recorded in the Cayman Trough (Leroy et al., 2000). This reconstruction assumed that the Chortis block moved along the WNW-ESE margin of southern Mexico, and rotated around the bend along the southern Maya block formed by the modern E-W striking Motagua fault during this time interval. This assumption led Boschman et al. (2014) to restore a counterclockwise rotation of ~30° after 50 Ma. A problem that arose in their reconstruction, and remained unsolved, is a 200–300 km overlap between the eastern part of Chortis, currently offshore, and the North Nicaraguan Rise in the Late Cretaceous. This overlap resulted from the restoration of Caribbean plate motion along the Belize (proto Swan Island) transform margin, and suggests that the restored position of Chortis in the Boschman et al. (2014) model at 50 Ma is not representative for the Late Cretaceous. Our new paleomagnetic data demonstrate that pre-50 Ma rotations affected the Chortis block, which now allows us to re-evaluate the pre-65 Ma kinematic evolution of Chortis.

In part, the overlap between Chortis and the Nicaraguan rise resulted because the Boschman et al. (2014) model treated the Nicaraguan Rise (Fig. 15) as a rigid tectonic unit, whereas Mann and Burke (1984) and recently Sanchez et al. (2016) reported evidence for post-Eocene east-west oriented extension on the Rise. Restoring such extension would already significantly decrease the overlap. Furthermore, the paleomagnetic results of the present study indicate that the Chortis block underwent a counterclockwise rotation that was ~55°, considerably larger than the ~30° angle between the southern Mexican margin and the Motagua fault assumed by Boschman et al. (2014). A

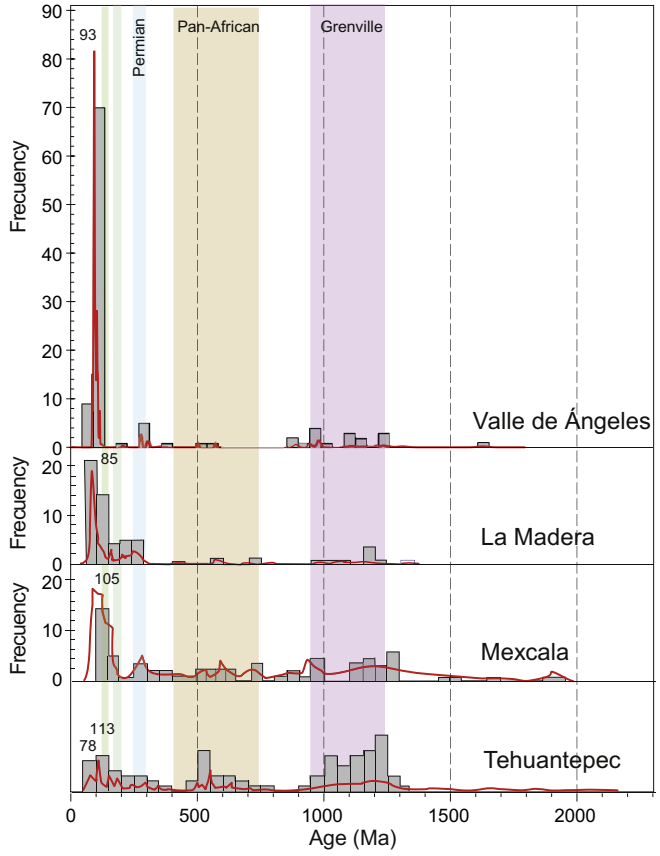

Fig. 16. Compilation of detrital zircon geochronology for Upper Cretaceous strata in southern Mexico compared with the Valle de Ángeles sample from the Frey Pedro Mountain area in Honduras.

straightforward geometrical consequence of this additional 25° of vertical axis rotation is that the Chortis block has not only experienced transform motion relative to North America, but must have undergone extension or contraction, depending on the location of the North America-Chortis Euler pole.

Two approaches can be used to estimate the North America-Chortis Euler pole during this rotation. In one scenario, a 70 Ma position of the northwestern tip of Chortis is determined by the location of the magnetic boundary in the Chortis block that is correlated to the Arperos suture in Mexico (Rogers et al., 2007a). Alternatively, an along-coast younging trend in ages of arc magmatism in southern Mexico in Paleocene to Neogene time has been interpreted to reflect the ESE-ward migration of the trench-trench-transform triple junction between the western North American and Central American trenches, and the (proto-) Motagua transform (e.g., Schaaf et al., 1995; Molina Garza et al., 2015). This migration was estimated at 1.2 cm/yr prior to 40 Ma, accelerating to 7.7 cm/yr after 40 Ma (Schaaf et al., 1995). This second approach would place the northwestern tip of Chortis a few tens of km farther north and west at 70 Ma than the approach of Rogers et al. (2007a). Given the similar results, we prefer the geological correlation of Rogers et al. (2007a), which we use to update the model of Boschman et al. (2014).

Reconstructing the 55° ccw rotation of Chortis around an Euler pole at the northwest Chortis-Mexico boundary opens a triangular gap between the northeastern margin of the Chortis block and southern Mexico with a maximum width of ~300 km. Such a restored gap must have been consumed by convergence during rotation of Chortis. The question now arises what the nature of this crust was. Clues to this come from folded and northward thrusted Upper Cretaceous sediments in the Tehuantepec area of southern Mexico (Fig. 15), that must be restored between Chortis and Mexico during their deposition and deformation in Late Cretaceous to Paleocene time. The Tehuantepec area exposes phyllite, carbonate rocks, chert, mafic volcanic rocks (both massive and pillows), and serpentinite slivers (Pérez-Gutiérrez et al., 2009). This assemblage suggests that the area consumed during rotation between Chortis and Mexico represents a highly extended, possibly oceanic basin. In any case, the Tehuantepec stratigraphy is considerably deeper marine than found on Chortis, and was not a continuation of the continental Chortis block. Flat REE patterns reported in geochemical data obtained from the Tehuantepec volcanic rocks suggest that these represent MORB lavas, with reported U-Pb ages of ~65 Ma (Pérez-Gutiérrez et al., 2009).

The geologic record of the southern Tehuantepec isthmus suggest that an extensional (or transtensional) basin formed behind (east of) the active arc related to Farallon subduction below Chortis; the basin opened between Oaxaca and Chortis until at least ~65 Ma. Because this area is recognized in Mexican geologic maps as the Chontal terrane (Carfantan, 1983), we refer to this basin as the Chontal basin. In addition, Talavera-Mendoza et al. (2013) have also interpreted the existence of a Late Cretaceous basin in the Xolapa terrane of the coastal Oaxaca margin based on detrital zircon geochronology of paragneises of the Xolapa Complex.

We hence restore the extensional opening of the Chontal basin to occur during deposition of it's deep-marine and mafic volcanic stratigraphy, ~80–65 Ma, by clockwise rotation of Chortis, such that a triangular basin opens in such a way that becomes smaller toward the northwest, where its remnants are not found. Besides the rotations of Chortis, we implemented 50 km of Paleogene-Neogene sinistral strike-slip motion on the Guayape fault, which was estimated to have accommodated strike-slip motion after the Late Cretaceous deposition of the Valle de Ángeles strata (Finch and Ritchie, 1991). New finite rotation poles for Chortis are provided in Supplementary Information 4.

Our paleomagnetic and stratigraphic constraints from Honduras suggest that the counterclockwise rotation of Chortis occurred roughly sometime after 70 Ma, and we therefore suggest that the counterclockwise rotation of Chortis resulted in closure of the Chontal basin and compression in the Chivela area of the Tehuantepec isthmus (Fig. 15), which recorded NNE directed compression consistent with our restoration (Pérez-Gutiérrez et al., 2009). NNE directed compression must have occurred between Eocene and Miocene time during the eastward migration of Chortis, since it was followed by Lower Miocene left-lateral strike-slip and Middle Miocene extension. Compression (or transpression) and strike-slip recorded after NNE compression are likely related to the eastward passage of Chortis (Molina Garza et al., 2012).

The stratigraphic and structural records of Tehuantepec had been previously interpreted as evidence of collision of the Greater Antilles arc against the Maya block of southern Mexico (the Chontal arc of Pindell et al., 2012). A similar interpretation was proposed by Pérez-Gutiérrez et al. (2009). The reconstruction of Chortis in the light of our new paleomagnetic constraints restores its western margin to a nearly north-south orientation, which makes these prior interpretations implausible. The record of Late Cretaceous-Paleocene compression and east-west strike slip in the Chivela area casts doubts on the claim of Keppie and Moran-Zenteno (2005) that the Tehuantepec area lacks a record of Late-Cretaceous-Cenozoic deformation, as well as their reconstruction of Chortis isolated from other continental blocks in the eastern Pacific. Our interpretation implies that the age assigned to undeformed conglomeratic sediments in the Tehuantepec area by Keppie and Moran-Zenteno (2005) is erroneous.

The stratigraphic documentation of pre-65 Ma subsidence and mafic volcanism, and by inference, extension or transtension because of the relative motion between the Caribbean and North America plates in the Chontal basin has an interesting implication for the subduction dynamics along the southwestern North American margin. The extension in the Chontal basin is located in the back-arc region of the Late Cretaceous volcanic arc that relates to the subduction of the Farallon

plate below Chortis and southern Mexico (Ferrari et al., 2014; Morán-Zenteno et al., 2017). This back-arc extension suggests that the Farallon slab subducting below the Chortis block underwent westward roll-back from an ill-defined moment of inception (modeled as 80 Ma) until ~65 Ma. This is interesting because the Farallon slab farther to the north is believed to have been a flat slab from ~85–55 Ma or even after that time, and responsible for significant North American plate shortening known as the Laramide orogeny (e.g., DeCelles et al., 2009; Fan and Carrapa, 2014). We envisage that the Farallon slab below Chortis had the freedom to roll back despite the flat slabs to the north, because of the trench-trench-transform triple junction that must have existed between the Farallon, Caribbean, and North American plate (Pindell and Kennan, 2009; Boschman et al., 2014). At this triple junction, the Farallon plate had a slab edge, around which toroidal flow may have accommodated roll-back at much higher rates than in the more interior parts of the slab farther north (see e.g. Schellart et al., 2007; Schepers et al., 2017). The kinematic history of the Chortis Block close to the NAM-CAR-FAR triple junction that we show in this paper may thus provide a straightforward explanation for the southern termination of the Laramide flat slab.

5. Conclusions

We sampled Cretaceous sediments on the Central Chortis terrane in Honduras for paleomagnetic and geochronological analysis. The Átima Limestone and redbeds of the Valle de Ángeles Formation of Cretaceous age carry multi-vectorial magnetizations. The ChRM is secondary, post-dating Late Cretaceous folding; the age of the magnetization is bracketed between about 85 and 63 Ma from the maximum depositional age and a cross-cutting undeformed dike. Five localities record west-northwest ChRMs of moderately positive inclination (mean $I = 39.7^{\circ}$), which averaged are interpreted to reflect 55° of counterclockwise rotation of the Chortis block relative to North America. Using these data, we restore the kinematic history of the Chortis block, currently part of the NW Caribbean plate, but in Cretaceous to Paleocene time part of the SW North American plate and located above the Farallon slab.

The stratigraphic and structural ties between southern Mexico and Chortis reported by Rogers et al. (2007a) are further strengthen by the interpretation of detrital zircon geochronology in Jurassic and Cretaceous strata. These data, together with our paleomagnetic data and the demonstrated continuity of the Laramide arc (Cenomanian-Turonian) from western Mexico into Chortis, strongly support the reconstruction of Chortis south of the (truncated) coast of southwestern Mexico. The reconstruction shows a triangular gap between Chortis and the Oaxaca continental margin prior to about 70 Ma. We proposed a model where the gap was formed by back-arc extension (or transtension). This process created the Chontal Upper Cretaceous basin, which reached a stage of ocean floor magmatism recorded in the southern Tehuantepec isthmus.

The opening and closure of the Chontal basin, and the associated vertical axis rotation of the Chortis block, shed interesting new light on the southern limit of the Farallon slab. Farallon is thought to have undergone flat subduction below North America between ~85–55 Ma. Plate reconstructions show that this slab must have had a slab edge south of Chortis at the triple junction with Caribbean plate boundaries. Toroidal flow at the southern termination of the Farallon slab may thus have facilitated back-arc extension in Tehuantepec through slab-roll back. Post 65 Ma motion of Chortis caused NNE directed compression and closure of the basin between Chortis and Oaxaca in the Tehuantepec region in the Eocene-Oligocene (Chivela fold and thrust system), and a record of Miocene left-lateral strike slip. Our study constrains the history of the Chortis block from its position at the southern termination of the Farallon/Laramide slab to its modern position incorporated as part of the Caribbean plate.

Acknowledgements

R.S.M.G. acknowledges funding through Consejo Nacional de Ciencia y Tecnología grant 129862. D.J.J.v.H. acknowledges funding through ERC Starting Grant 306810 (SINK) and NWO VIDI grant 864.11.004. LMB acknowledges NWO grant 824.01.004. We thank Cor Langereis for discussion.

Appendix A. Supplementary data

Supplementary data to this article can be found online at https://doi.org/10.1016/j.tecto.2017.11.026.

References

Acton, G.D., Galbrun, B., King, J.W., 2000. Paleolatitude of the Caribbean plate since the Late Cretaceous. Proc. Ocean Drill. Program Sci. Results 165, 149–173.
Bird, P., 1988. Formation of the Rocky Mountains, western United States: a continuum computer model. Science 239, 1501–1507.
Böhnel, H., Alva, L., González, S., Urrutia, J., Morán, D., Schaaf, P., 1989. Paleomagnetic data and the accretion of the Guerrero terrane, southern México continental margin. In: Hillhouse, J.W. (Ed.), Deep Structure and Past Kinematic of Accreted Terranes. 5. AGU Geophysical Monograph/I.U.G.G., pp. 73–92.
Boschman, L.M., van Hinsbergen, D.J.J., Torsvik, T.H., Spakman, W., Pindell, J.L., 2014. Kinematic reconstruction of the Caribbean region since the Early Jurassic. Earth Sci. Rev. 138, 102–136.
Campos Madrigal, E., Centeno-García, E., Mendoza-Rosales, C.C., Silva-Romo, G., 2013. Sedimentología, reconstrucción paleoambiental y significado tectónico de las sucesiones clásticas del Jurásico Medio en el área de Texcalapa, Puebla-Huajuapan de León, Oaxaca: Revisión de las formaciones Ayuquila y Tecomazúchil. Rev. Mexicana Ciencias Geológicas 30, 24–50.
Carfantan, J.C., 1983. Les ensambles géologiques du Mexique méridional – Évolution geodynamique durant le Mészoïque et le Cenozoïque. Geofis. Int. 22, 9–37.
Case, J.E., Holcombe, T.L., 1980. Geologic-tectonic map of the Caribbean region, Reston, Virginia. In: United States Geological Survey.
Corona-Chávez, P., Poli, S., Biogioggero, B., 2006. Syn-deformational migmatites and magmatic arc metamorphism in the Xolapa complex, southern Mexico. J. Metam. Geol. 24, 169–191.
DeCelles, P.G., Ducea, M.N., Kapp, P., Zandt, G., 2009. Cyclicity in Cordilleran orogenic systems. Nat. Geosci. 2, 251–257.
Deenen, M.H.L., Langereis, C.G., van Hinsbergen, D.J.J., Biggin, A.J., 2011. Geomagnetic secular variation and the statistics of palaeomagnetic directions. Geophys. J. Int. 186, 509–520.
Dengo, G., 1969. Problems of tectonic relations between Central America and the Caribbean. In: GCAGS Transactions, pp. 19. http://dx.doi.org/10.1306/A1ADF38F-0DFE-11D7-8641000102C1865D.
Dengo, G., 1985. Mid America; tectonic setting fro the Pacific margin from southern Mexico to northwestern Colombia. In: Nairn, A.E.M., Stehli, F.G. (Eds.), Ocean Basins and Margins 7. Plenum Press, New York, pp. 123–180.
Dickinson, W.R., Gehrels, G.E., 2009. U-Pb ages of detrital zircons in Jurassic eolian and associated sandstones of the Colorado Plateau: evidence for transcontinental dispersal and intraregional recycling of sediment. Geol. Soc. Am. Bull. 121, 408–433.
Fan, M., Carrapa, B., 2014. Late cretaceous-early Eocene Laramide uplift, exhumation, and basin subsidence in Wyoming: crustal responses to flat slab subduction. Science 33, 509–529. http://dx.doi.org/10.1002/2012TC003221.
Ferrari, L., Bergomi, M., Martini, M., Tunesi, A., Orozco-Esquivel, T., López-Martínez, M., 2014. Late Cretaceous-Oligocene magmatic record in southern Mexico: the case for a temporal slab window along the evolving Caribbean-North America-Farallon triple boundary. Tectonics 33, 1738–1765.
Finch, R.C., Ritchie, A.W., 1991. The Guayape fault system, Honduras, Central America. J. South Am. Earth Sci. 4, 43–60.
Fitz-Díaz, E., Hudleston, P., Tolson, G., 2011. Comparison of tectonic styles in the Mexican and Canadian Rocky Mountain fold-Thrust Belt. Geol. Soc. Lond. Spec. Publ. 349, 149–167.
Flores, K.E., Skora, S., Martin, C., Harlow, G.E., Rodríguez, D., Baumgartner, P.O., 2015. Metamorphic history of riebeckite- and aegirine-augite-bearing high-pressure–low-temperature blocks within the Siuna Serpentinite Mélange, northeastern Nicaragua. Int. Geol. Rev. 57 (5–8), 943–977.
García-Casco, A., Iturralde-Vinent, M.A., Pindell, J., 2008. Latest cretaceous collision/accretion between the caribbean plate and caribeana: origin of metamorphic terranes in the greater antilles. Int. Geol. Rev. 50, 781–809.
Gordon, M.B., 1993. Revised Jurassic and Early Cretaceous (Pre-Yojoa Group) stratigraphy of the Chortis block: Paleogeographic and tectonic implications. In: Pindell, J.L., Perkins, R.F. (Eds.), Mesozoic and Early Cenozoic Development of the Gulf of Mexico and Caribbean Region: a Context for Hydrocarbon Exploration. Gulf Coast Section Society of Economic Paleontologists and Mineralogists Foundation, Austin. Texas, pp. 143–154.
Gose, W., 1985. Paleomagnetic results from Honduras and their bearing on Caribbean tectonics. Tectonics 4, 565–585.
Gose, W., Finch, R.C., 1992. Stratigraphic implications of palaeomagnetic data from Honduras. J. Geophys. Res. 108, 855–864.

Herrmann, U.R., Nelson, B.K., Ratschbacher, L., 1994. The origin of a terrane: U/Pb zircon geochronology and tectonic evolution of the Xolapa complex (southern Mexico). Tectonics 13, 455–474.
Horne, G., Clark, G., Pushkar, P., 1976. Pre-cretaceous rocks of northwestern Honduras: Basement terrane in Sierra de Omoa. AAPG Bull. 60, 566–583.
Keppie, D.F., Keppie, J.D., 2012. An alternative Pangea reconstruction for Middle America with the Chortis Block in the Gulf of Mexico: tectonic implications. Int. Geol. Rev. http://dx.doi.org/10.1080/00206814.2012.676361.
Keppie, J.D., Moran-Zenteno, D.J., 2005. Tectonic implications of alternative Cenozoic reconstructions for Southern Mexico and the Chortis block. Int. Geol. Rev. 47, 473–491.
Kirschvink, J.L., 1980. The least-squares line and plane and the analysis of paleomagnetic data: examples from Siberia and Morroco. Geophys. J. Roy. Astron. Soc. 62, 699–718.
Koymans, M.R., Langereis, C.G., Pastor-Galán, D., van Hinsbergen, D.J.J., 2016. Paleomagnetism.org: an online multi-platform open source environment for paleomagnetic data analysis. Comput. Geosci. 93, 127–137.
Lázaro, C., García-Casco, A., Rojas Agramonte, Y., Kröner, A., Neubauer, F., Iturralde-Vinent, M.A., 2009. Fifty-five-million-year history of oceanic subduction and exhumation at the northern edge of the Caribbean plate (Sierra del Convento mélange, Cuba). J. Metamorph. Geol. 27 (1), 19–40. http://dx.doi.org/10.1111/j.1525-1314.2008.00800.x.
Leroy, S., Mauffret, A., Patriat, P., Mercier de Lépinay, B., 2000. An alternative interpretation of the Cayman trough evolution from a re-identification of magnetic anomalies. Geophys. J. Int. 141, 539–557.
Liu, L., Gurnis, M., Seton, M., Saleeby, J., Müller, R.D., Jackson, J.M., 2010. The role of oceanic plateau subduction in the Laramide orogeny. Nat. Geosci. 3 (5), 353–357. http://dx.doi.org/10.1038/ngeo829.
Mann, P., 2007. Overview of the tectonic history of northern Central America. GSA Special Papers 428, 1–19. http://dx.doi.org/10.1130/2007.2428(01).
Mann, P., Burke, K., 1984. Neotectonics of the Caribbean. Rev. Geophys. 22 (4), 309–362.
Manton, W., 1996. The Grenville of Honduras. In: Geological Society of America Abstracts with Programs. 28. pp. A-493.
McFadden, P.L., 1990. A new fold test for palaeomagnetic studies. Geophys. J. Int. 103, 163–169.
McFadden, P.L., McElhinny, M.W., 1990. Classification of the reversal test in palaeomagnetism. Geophys. J. Int. 103, 725–729.
McFadden, P.L., Reid, A.B., 1982. Analysis of palaeomagnetic inclination data. Geophys. J. R. Astron. Soc. 69, 307–319.
Meschede, M., Frisch, W., 1998. A plate-tectonic model for the Mesozoic and Early Cenozoic history of the Caribbean plate. Tectonophysics 296, 269–291.
Molina Garza, R.S., van Hinsbergen, D.J.J., Rogers, R.D., Ganerød, M., Dekkers, M.J., 2012. The Padre Miguel Ignimbrite suite, central Honduras: Paleomagnetism, geochronology, and tectonic implications. Tectonophysics 574-575, 144–157.
Molina Garza, R.S., Geissman, J.W., Wawtzyniec, T.F., Peña Alonso, T.A., Iriondo, A., Weber, B., Aranda-García, J.J., 2015. Geology of the coastal Chiapas (Mexico) Miocene plutons and the Tonalá shear zone: syntectonic emplacement and rapid exhumation during sinistral transpression. Lithosphere 7, 257–274. http://dx.doi.org/10.1130/L409.1.
Molina-Garza, R.S., Böhnel, H.N., Hernández, T., 2003. Paleomagnetism of the Cretaceous Morelos and Mexcala formations, southern Mexico. Tectonophysics 361 (3), 301–317.
Morán-Zenteno, D.J., Martiny, B.M., Solari, L., Mori, L., Luna-González, L., González-Torres, E.A., 2017. Cenozoic magmatism of the Sierra Madre del Sur and tectonic truncation of the Pacific margin of southern Mexico. Earth Sci. Rev. http://dx.doi.org/10.1016/j.earscirev.2017.01.010.
Mullender, T.A.T., Frederichs, T., Hilgenfeldt, C., de Groot, L.V., Fabian, K., Dekkers, M.J., 2016. Automated paleomagnetic and rock magnetic data acquisition with an in-line horizontal "2G" system. Geochem. Geophys. Geosyst. 17, 3546–3559. http://dx.doi.org/10.1002/2016GC006436.
Peña-Alonso, T.A., Estrada-Carmona, J., Molina-Garza, R.S., Solari, L., Levresse, G., Latorre, C., 2017. Lateral spreading of the middle to lower crust inferred from Paleocene migmatites in the Xolapa complex (Puerto Escondido, Mexico): gravitational collapse of a Laramide orogen? Tectonophysics 706–707, 143–163.
Pérez-Gutiérrez, R., Solari, L.A., Gómez-Tuena, A., Valencia, V.A., 2009. El terreno Cuicateco: ¿cuenca oceánica con influencia de subducción del Cretácico Superior en el sur de México? Nuevos datos estructurales, geoquímicos y geocronológicos. Rev. Mexicana de Ciencias Geológicas 26, 222–242.
Pindell, J.L., Barrett, S.F., 1990. Geological evolution of the Caribbean region; a plate-tectonic perspective. In: Boulder, Geological Society of America, The geology of North America. H, pp. 405–432.
Pindell, J., Kennan, L., 2009. Tectonic evolution of the Gulf of Mexico, Caribbean and northern South America in the mantle reference frame: an update. In: James, K., Lorente, M.A., Pindell, J. (Eds.), The geology and Evolution of the Region Between North and South America. Geological Society of London Special Publication 328. pp. 1–57.
Pindell, J.L., Maresch, W.V., Martens, U., Stanek, K.P., 2012. The greater Antillean arc: early Cretaceous origin and proposed relationship to Central American subduction mélanges: implications for models of Caribbean evolution. Int. Geol. Rev. 54, 131–143.
Ratschbacher, L., Riller, U., Meschede, M., Herrmann, U., Frisch, W., 1991. Second look at suspect terranes in southern Mexico. Geology 19, 1233–1236.
Ratschbacher, L., Franz, L., Min, M., Bachmann, R., Martens, U., Stanek, K., Stübner, K., Nelson, B.K., Herrmann, U., Weber, B., López-Martínez, M., Jonckheere, R., Sperner, B., Tichomirowa, M., Mcwilliams, M.O., Gordon, M., Meschede, M., Bock, P., 2009. The North American-Caribbean plate boundary in Mexico-Guatemala-Honduras. Geol. Soc. Lond. Spec. Publ. 328, 219–293.
Finch, R.C., 1981. Mesozoic stratigraphy of central Honduras. AAPG Bull. 65, 1620–1633.
Riller, U., Ratschbacher, L., Frisch, W., 1992. Left-lateral transtension along the Tierra Colorada deformation zone, northern margin of the Xolapa magmatic arc of southern Mexico. J. S. Am. Earth Sci. 5, 237–249.
Rogers, R.D., Mann, P., Emmet, P.A., 2007a. Tectonic terranes of the Chortis block based on integration of regional aeromagnetic and geologic data. In: GSA Special Paper 428. pp. 65–88.
Rogers, R.D., Mann, P., Emmet, P., Venable, M., 2007b. Colon fold-thrust belt of Honduras: evidence for late cretaceous collision between the continental Chortis block and intra-oceanic Caribbean arc. In: GSA Special Paper 428. pp. 129–149.
Rogers, R.D., Mann, P., Scott, R.W., Patino, L., 2007c. Cretaceous intra-arc rifting. In: GSA Special Paper 428. pp. 89–128.
Ross, M.I., Scotese, C.R., 1988. A hierarchical tectonic model of the Gulf of Mexico and Caribbean region. Tectonophysics 155, 139–168. http://dx.doi.org/10.1016/0040-1951(88)90263-6.
Sanchez, J., Mann, P., Emmet, P.A., 2016. Late Cretaceous-Cenozoic tectonic transition from collision to transtension, Honduras borderlands and Nicaragua Rise, NW Caribbean Plate boundary. Geol. Soc. Lond. Spec. Publ. 431, 273–297.
Sánchez-Zavala, J.L., Ortega-Gutiérrez, F., Keppie, J.D., Jenner, G.A., Belousova, E., Macías-Romo, C., 2004. Ordovician and Mesoproterozoic zircons from the Tecomate formation and Esperanza Granitoids, Acatlán Complex, Southern Mexico: local provenance in the Acatlán and Oaxacan complexes. Int. Geol. Rev. 46, 1005–1021.
Schaaf, P., Morán-Zenteno, D., Hernández-Bernal, M.S., 1995. Paleogene continental margin truncation in southwestern Mexico: Geochronological evidence. Tectonics 14, 1229–1350.
Schellart, W.P., Freeman, J., Stegman, D.R., Moresi, L., May, D., 2007. Evolution and diversity of subduction zones controlled by slab width. Nature 446 (7133), 308–311. http://dx.doi.org/10.1038/nature05615.
Schepers, G., van Hinsbergen, D.J., Kosters, M.E., Boschman, L.M., McQuarrie, N., Spakman, W., 2017. South American plate advance and forced trench retreat as drivers for transient Andean flat subduction episodes. Nat. Commun. http://dx.doi.org/10.1038/ncomms15249.
Sierra-Rojas, M.I., Molina-Garza, R.S., Lawton, T.F., 2016. The Aptian Atzompa formation in south central Mexico: record of evolution from extensional back-arc basin margin to carbonate platform. J. Sediment. Res. 86, 712–733.
Silva-Romo, G., 2008. Guayape-Papalutla fault system: a continuous Cretaceous structure from southern Mexico to the Chortís block? Tectonic implications. Geology 36, 75–78.
Simonson, B., 1977. Mapa geológico de Honduras, El Porvenir. Instituto Geográfico Nacional, Tegucigalpa (scale 1:50,000).
Talavera-Mendoza, O., Ruiz, J., Gehrels, G.E., Meza-Figueroa, D.M., Vega-Granillo, R., Campa-Uranga, M.F., 2005. U–Pb geochronology of the Acatlán complex and implications for the Paleozoic paleogeography and tectonic evolution of southern Mexico. Earth Planet. Sci. Lett. 235, 682–699.
Talavera-Mendoza, O., Ruiz, J., Gehrels, G.E., Valencia, V.A., Centeno-García, E., 2007. Detrital zircon U/Pb geochronology of southern Guerrero and western Mixteca arc successions (southern Mexico): New insights for the tectonic evolution of southwestern North America during the late Mesozoic. Geol. Soc. Am. Bull. 119, 1052–1065.
Talavera-Mendoza, O., Ruiz, J., Corona-Chavez, P., Gehrels, G.E., Sarmiento-Villagrana, A., García-Díaz, J.L., Salgado-Souto, S.A., 2013. Origin and provenance of basement metasedimentary rocks from the Xolapa Complex: New constraints on the Chortis–southern Mexico connection. Earth Planet. Sci. Lett. 369–370, 188–199.
Tauxe, L., 2010. Essentials of Paleomagnetism. University of California Press 529 pp.
Tauxe, L., Watson, G.S., 1994. The fold test: an eigenvalue approach. Earth Planet. Sci. Lett. 122, 331–341.
Torsvik, T.H., Müller, R.D., Van der Voo, R., Steinberger, B., Gaina, C., 2008. Global plate motion frames: toward a unified model. Rev. Geophys. 41, RG3004. http://dx.doi.org/10.1029/2007RG000227.
Van der Voo, R., 1990. The reliability of paleomagnetic data. Tectonophysics 184, 1–9.
Zijderveld, J.D.A., 1967. A. C. demagnetization of rocks - analysis of results. In: Collinson, D.W., Creer, K.M., Runcorn, S.K. (Eds.), Methods in Rock Magnetism and Paleomagnetism. Elsevier, Amsterdam, Netherlands, pp. 254–286.